

# How Cosmic Web Detachment Drives Galaxy Quenching

Miguel A. Aragon-Calvo<sup>1\*</sup>, Mark C. Neyrinck<sup>2,3,4</sup>, Joseph Silk<sup>2,3,4,5</sup>

<sup>1</sup>*Department of Physics and Astronomy, University of California, Riverside, 900 University Ave, Riverside, CA 92521, USA*

<sup>2</sup>*Department of Physics and Astronomy, The Johns Hopkins University, Baltimore, MD 21218, USA*

<sup>3</sup>*Sorbonne Universites, UPMC Univ Paris 6 et CNRS, UMR 7095, Institut d'Astrophysique de Paris, 98 bis bd Arago, F-75014 Paris, France*

<sup>4</sup>*AIM-Paris-Saclay, CEA/DSM/IRFU, CNRS, Univ Paris 7, F-91191, Gif-sur-Yvette, France*

<sup>5</sup>*BIPAC, University of Oxford, 1 Keble Road, Oxford OX1 3RH, UK*

## ABSTRACT

We present the Cosmic Web Detachment (CWD) model, a conceptual framework to interpret galaxy evolution in a cosmological context, providing a direct link between the star formation history of galaxies and the cosmic web. The CWD model unifies several mechanism known to disrupt or stop star formation into one single physical process and provides a natural explanation for a wide range of galaxy properties. Galaxies begin accreting star-forming gas at early times via a network of *primordial* highly coherent filaments. The efficient star formation phase ends when non-linear interactions with other galaxies or elements of the cosmic web *detach* the galaxy from its network of primordial filaments, thus ending the efficient accretion of cold gas. The stripping of the filamentary web around galaxies is the physical process responsible of star formation quenching in gas stripping, harassment, strangulation and starvation. Being a purely gravitational/mechanical process CWD acts at a more fundamental level than internal feedback processes.

We introduce a simple and efficient formalism to identify CWD events in N-body simulations. With it we reproduce and explain, in the context of CWD, several key observations including downsizing, the cosmic star formation rate history, the galaxy mass-color diagram and the dependence of the fraction of red galaxies with mass and local density.

**Key words:** Cosmology: large-scale structure of Universe; galaxies: kinematics and dynamics; methods: data analysis, N-body simulations

## 1 INTRODUCTION

Star formation quenching, its underlying mechanism and what triggers it, is one of the most pressing problems in modern galaxy formation. Galaxies in the Universe are either actively forming stars or in a “quenched” state of practically no star formation. This dichotomy is reflected in the bi-modality in the color-magnitude diagram (Strateva et al. 2001; Hogg et al. 2004; Baldry et al. 2004; Faber et al. 2007; Schiminovich et al. 2007) clearly separating blue star-forming spiral galaxies from red “quenched” elliptical galaxies (see Dekel & Birnboim (2006a) for a review). Most galaxies sit in one of the two groups and only a few galaxies are found in the “green valley” in between (Schawinski et al. 2014). The clear gap between the two galaxy populations can be interpreted as star formation quenching either having occurred several Gyr ago

and/or that it is a fast event (Bell et al. 2004; Blanton 2006; Wyder et al. 2007; Salim et al. 2007).

Several mechanism have been proposed as responsible for the decrease in star formation activity in galaxies. Currently favored candidates include internal feedback processes such as AGN and supernovae feedback (Silk & Rees 1998; Di Matteo, Springel & Hernquist 2005; Best et al. 2005). However, the non-causal connection between black hole mass vs. bulge mass challenges the predominant place given to AGN in galaxy formation (Peng 2007; Jahnke & Macciò 2011) allowing other options. Cosmic environment has been long recognized as playing a major role shaping the properties of galaxies, specially in dense environments, in the form of ram pressure and gas stripping (Gunn & Gott 1972; Balsara, Livio & O’Dea 1994; Abadi, Moore & Bower 1999; Quilis, Moore & Bower 2000; Hester 2006; McCarthy et al. 2008), harassment (Moore et al. 1996; Moore, Lake & Katz 1998), strangulation (Bekki, Couch & Shioya 2002; Fujita 2004;

\* E-mail: maragon@ucr.edu

Kawata & Mulchaey 2008; Peng, Maiolino & Cochrane 2015), preprocessing (Kodama & Bower 2001; Treu et al. 2003; Goto et al. 2003; Fujita 2004). These processes have in common that they are external influences that affect star formation by preventing gas from reaching galaxies or by removing gas reservoirs. Recent studies show environmentally induced quenching independent of AGN feedback from purely geometric constraints (Aragon-Calvo, Neyrinck & Silk 2014) and an undefined but clear cosmological origin (Feldmann & Mayer 2015; Peng, Maiolino & Cochrane 2015). The spacial correlation of galaxy properties, up to scales of several megaparsecs, also points to the dominant role of environment on galaxy evolution (Dressler 1980; Weinmann et al. 2006; Kauffmann et al. 2013).

Both observations and simulations point to star formation quenching being the result of environmental (external) processes and feedback (internal) processes (Hogg et al. 2003; Blanton et al. 2005; Cooper et al. 2007; Coil et al. 2008; Peng et al. 2010; van de Voort et al. 2011) but their relative importance is not clear yet. External processes are usually characterized by local density, a first-order environmental descriptor with limited power to encode the intricate geometry of the cosmic web crucial to understand the geometry and dynamics of gas accretion, galaxy interactions, etc. Internal processes seem to be driven by halo mass (Peng et al. 2010). However, halo mass and density are correlated, making this relation not straightforward to interpret.

### 1.1 The need for a cosmic web-based galaxy formation model

Current galaxy formation models, in particular semi-analytical implementations, can reproduce a wide range of observations and provide useful insight on the physical processes occurring inside galaxies (Rees & Ostriker 1977; White & Rees 1978; Lacey & Silk 1991; Cole 1991; White & Frenk 1991; Kauffmann, White & Guiderdoni 1993; Somerville & Primack 1999; Cole et al. 2000; Benson et al. 2001, 2002; Hatton et al. 2003; Monaco, Fontanot & Taffoni 2007; Somerville et al. 2008). These models intrinsically consider galaxies as isolated entities and interactions with other galaxies and their cosmic environment are only indirectly treated via their mass accretion and merger history (Hearin & Watson 2013; Mutch, Croton & Poole 2013; Hearin et al. 2014; Rodríguez-Puebla et al. 2016). The accretion/merger history of galaxies is insensitive to the particular geometry and dynamics of the cosmic web surrounding galaxies. However, there is extensive evidence of the effect of cosmic environment (beyond the traditional cluster vs. field separation) on halo/galaxy properties (Navarro, Abadi & Steinmetz 2004; Trujillo, Carretero & Patiri 2006; Aragón-Calvo et al. 2007b,a; Hahn et al. 2007; Darvish et al. 2014; Chen et al. 2015; Alpaslan et al. 2016; Darvish et al. 2016). For instance, star-forming gas is tunneled into the cores of early galaxies via a network of dense filamentary streams (Dekel et al. 2009) but this key information is not included in current galaxy formation models making them blind to environmental effects on the filamentary streams, one of the main paths for gas accretion in galaxies.

A semi-analytic model relevant to the one presented here is the empirical *age matching* approach (Hearin & Watson 2013; Hearin et al. 2014; Watson et al. 2015) (see also Rodríguez-Puebla et al. 2016, for another method based on mass accretion) in which the time for star formation quenching is assumed to be the first of i) the time when a galaxy reaches  $10^{12} h^{-1} M_{\odot}$ , ii) the formation time of the halo defined as the time when the slope in the mass accretion history changes and iii) the time when the halo is accreted into a larger halo, becoming a satellite. The *age* of the halo computed as above is then matched with observed properties of galaxies associated with time evolution such as color. Age matching is an empirical model which, despite being based on ad-hoc rules, can reproduce several observations (Hearin et al. 2014). However it does not explain the physical underlying process that define the age of a galaxy and so its explanatory and predictive power is limited. A successful theory of galaxy formation must be able to not only reproduce a range of observations but to provide a unifying framework that can explain and predict properties of galaxies.

### 1.2 Star-forming gas accretion via primordial filaments

Galaxy formation is a complex process that began when, driven by gravity, nodes of a tenuous web of primordial filaments emerged from tiny density fluctuations (Zel'dovich 1970), (see also Hidding, Shandarin & van de Weygaert 2014). At the nodes of this cosmic network proto-galaxies began to grow feeding via coherent filamentary streams of cold ( $T < 10^5 K$ ) gas (Kereš et al. 2005; Dekel et al. 2009; Danovich et al. 2012; Harford & Hamilton 2016). The coherence of the streams at early times makes gas accretion highly efficient. At  $z \sim 2$  most of the gas in star-forming galaxies is accreted via dense narrow filamentary streams that inject cold gas into the inner regions of galaxies even in the presence of shock heating (Dekel et al. 2009; Faucher-Giguère & Kereš 2011). In comparison, far less gas is accreted via the inefficient, isotropic, hot ( $T > 10^5 K$ ) accretion mode.

The nature of the cold streams connected to a proto-galaxy is closely linked to its surrounding matter distribution, and in particular to surrounding peaks, as described in the *Cosmic Web theory* (Bond, Kofman & Pogosyan 1996). The quadrupolar tidal field configuration associated to a pair of peaks results in the formation of a bridge of matter in between. The Cosmic Web theory is usually invoked to explain the large megaparsec-scale filaments observed in the galaxy distribution. However, the same principle can be applied at smaller scales and earlier times to describe the formation of bridges between proto-galaxies. Primordial filaments form from a nearly Gaussian field in a gravitationally young environment characterized by a highly coherent velocity field. Figure 1 shows a comparison between the density and velocity fields at  $z = 5$  and  $z = 0$ . The velocity field was high-pass filtered at 125 kpc in order to highlight dynamics on galactic scales instead of the large-scale flows that dominate the raw velocity field (see Aragón-Calvo & Szalay (2013) for details). The differences between the early and latter velocity fields are remarkable. The velocity field at  $z = 5$  is laminar and closely follows the filamentary net-

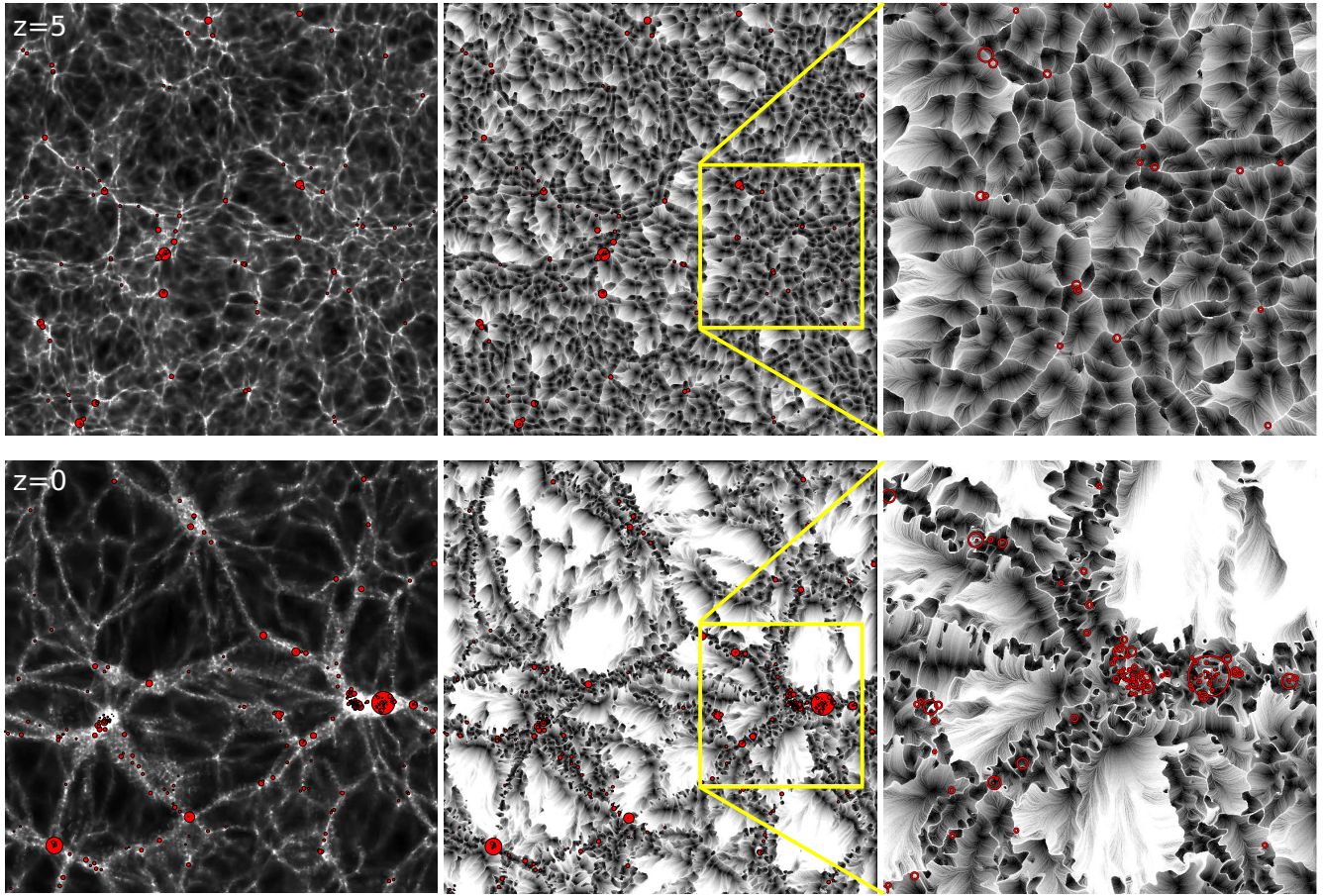


**Figure 1.** Coherent vs. turbulent velocity field around haloes. Left: a  $1 \text{ h}^{-1} \text{ Mpc}$  thick slice through the density field of a  $32 \text{ h}^{-1} \text{ Mpc}$  box. Center: the velocity field at scales smaller than  $125 \text{ h}^{-1} \text{ kpc}$  highlighted using the particle advection visualization technique (see Aragon-Calvo & Szalay 2013, for a description of the particle advection technique). The streams indicate the direction of the velocity field. The areas regions correspond to regions where the velocity field converges. Right: a zoomed region showing details in the velocity field. The red/white circles correspond to sub-haloes inside the slice. Top panels show that the velocity field at early times is highly coherent and closely delineates the location of primordial filaments connected to haloes. At latter times (bottom panels) the velocity field is highly turbulent and haloes are not connected to the observed streams.

work surrounding haloes. All haloes can be seen either at the nodes or ridges of the coherent structures (where the advected trajectories converge) in the velocity field. In contrast, the velocity field around haloes at  $z = 0$  is dominated by turbulent flows that do not correlate with haloes. As shown in Aragon-Calvo & Szalay (2013) the magnitude of the velocity field at small scales characteristic of the primordial velocity field are one order of magnitude smaller than the large-scale flows seen in the large present-time filaments. A typical example of such structures is the Pisces-Perseus ridge (Wegner, Haynes & Giovanelli 1993) spanning tens of megaparsecs and intersecting several galaxy groups and clusters. The different dynamical regimes between primordial and non-linear filaments has not been explicitly noted before and it is key for our understanding of gas accretion. Note that at  $z = 0$  there are practically no streams connected to haloes as in the case of  $z = 5$  where every halo is located at the position of one or multiple streams.

Figure 1 shows two different kinds of structures in the cosmic web separated by their gravitational evolutionary stage. Primordial filaments are formed immediately after haloes begin their collapse and have a marked cellular

nature and coherent velocity flows at small scales. The large filaments we see in the present-time galaxy distribution formed hierarchically by the collapse of smaller primordial filaments. They are larger, more massive and dynamically complex. Such large-scale structures also form a cellular system but at scales of tens of megaparsecs (Joeveer & Einasto 1978; Klypin & Shandarin 1983; Geller & Huchra 1989; Icke & van de Weygaert 1991; Aragon-Calvo, van de Weygaert & Jones 2010; Einasto et al. 2011; Aragon-Calvo & Szalay 2013; Aragon-Calvo, Neyrinck & Silk 2014). Present-time voids may still contain primordial filaments due to their super-Hubble expansion which freezes the development of structure at large scales. Such small-scale filaments are prevalent in high-resolution computer simulations of voids (Gottlöber et al. 2003; Sheth & van de Weygaert 2004; Park & Lee 2009; Aragon-Calvo & Szalay 2013; Rieder et al. 2013) and recently have been observed in deep surveys (Kreckel et al. 2012; Beygu et al. 2013; Alpaslan et al. 2014).

Figure 1 highlights the interplay between haloes and their surrounding cosmic web as a function of time and halo



mass (since the halo mass function is also a function of time). At  $z = 5$  the non-linear mass  $M_*$  is of the order of  $10^7 h^{-1} M_\odot$  while at the present time it is close to  $10^{13} h^{-1} M_\odot$  (see Fig. A1). The non-linear mass gives us a rough estimate of the mass-scale at which haloes become the dominant component of their surrounding cosmic web (Dekel et al. 2009). Haloes with masses larger than  $M_*$  are nodes of their local cosmic web while haloes less massive will be embedded inside a larger cosmic web element such as the case of galaxies in large filaments at the present time.

### 1.3 The fate of cold flows and star formation quenching

The stark difference in the velocity field around haloes at early and latter times gives us a clue on the fate of the primordial filaments feeding galaxies. The velocity field around haloes in present-time over-dense regions has no memory of the primordial filaments originally connected to the haloes as the result of non-linear dynamics. If gas accretion through coherent cold filamentary flows is the most efficient mechanism to inject star-forming gas into galaxies then we should see a clear change in star formation in haloes entering non-linear regions. The change in the accretion mode should be fast (within a few Gyr) given the efficient gas-star conversion of cold gas (Dekel et al. 2009; van de Voort et al. 2011) which makes a gas-starved galaxy stop producing stars within a short time scale (Bauermeister, Blitz & Ma 2010; Peng, Maiolino & Cochrane 2015). Based in our current knowledge of the relation between galaxies, star formation and gas accretion via cold flows we can enumerate the following key assertions:

- Proto-galaxies are the nodes of a network of primordial filaments.
- Star-forming cold gas is accreted mainly via primordial coherent filamentary streams.
- Star formation closely follows cold gas accretion and ends (to a first approximation) when the gas supply is cut.

These observations point to a process behind the drop in star formation that acts by affecting the gas infall through primordial filaments. Any mechanism that is able to separate a galaxy from its web of primordial filaments results in star formation quenching.

### 1.4 Filament detachment by accretion into a cluster

The results presented in this section are based on a zoom simulation from a  $64h^{-1}\text{Mpc}$  box. The zoom region is centered in a  $2.4 \times 10^{14} h^{-1} M_\odot$  cluster and has a mass resolution of  $2 \times 10^7 h^{-1} M_\odot$  per dark matter particle. The simulation includes gas with cooling and metal enrichment as well as stochastic star formation (see Appendix B).

Figure 2 shows a satellite galaxy being accreted into a large cluster with present-time masses of  $2 \times 10^{11} h^{-1} M_\odot$  and  $2.4 \times 10^{14} h^{-1} M_\odot$  respectively. This is a case of an extreme interaction between a galaxy and its environment that might be described as ram-pressure gas stripping (Mori & Burkert 2000; Quilis, Moore & Bower 2000; Mayer et al. 2006; Kronberger et al. 2008; Boselli et al.

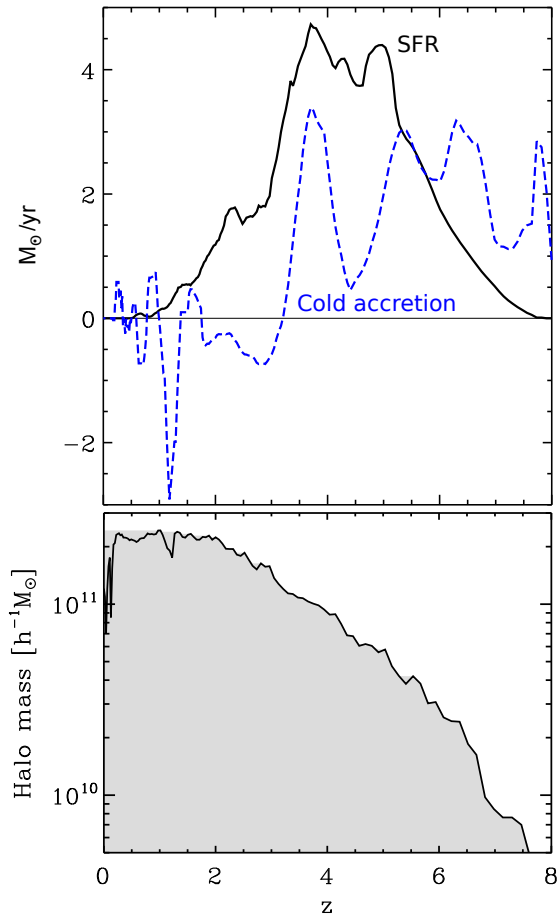


**Figure 3.** Top: cold gas accretion (dashed blue line) and star formation rate (solid black line) as a function of redshift, measured inside a shell of radius  $r_{vir} - 1.5r_{vir}$  centered in the halo presented in Fig. 2. Bottom: mass accretion history. The black line is the raw MAH and the solid area the fixed MAH as described in the text.

2008; De Rijcke, Van Hese & Buyle 2010), and clearly shows non-linear effects not only on the galaxy but on its surrounding network of filaments. As the galaxy begins to interact with the cluster we see changes in its surrounding matter configuration, mass accretion and star formation.

The top panels in Fig. 2 show that at early times ( $z = 5$ ) the satellite galaxy is the central node of a network of thin filaments. The filaments were identified by placing test particles and letting them follow the instantaneous velocity field interpolated using a Delaunay tessellation linear interpolation scheme (Schaap & van de Weygaert 2000) and applying a high-pass filter at the scale of interests (Aragon-Calvo & Szalay 2013). The places where the particles accumulate were used to construct a filament mask which was then used to tag particles in the simulation (Aragon-Calvo in preparation). The corresponding velocity field is composed of coherent filamentary streams of gas and dark matter that delineate the location of the primordial filaments in the matter distribution. It is worth noting that the (high-pass filtered) velocity field shows the filamentary structures in the cosmic web more clearly than the density field. The coherent filamentary structures in the velocity field at  $z = 5$  have a laminar character re-

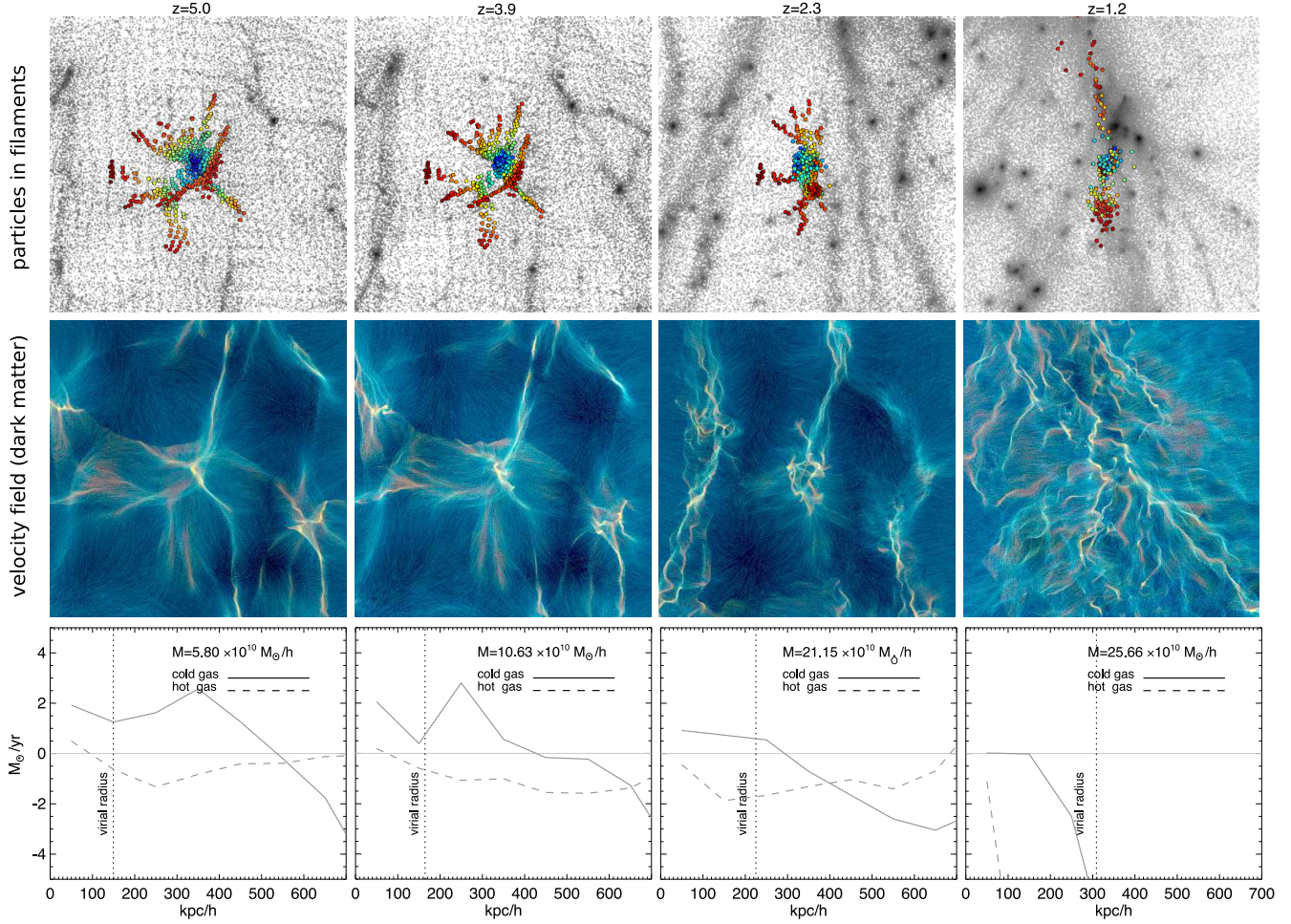


**Figure 2. Web Detachment of a  $2.3 \times 10^{11} h^{-1} M_\odot$  galaxy by accretion into a  $2.4 \times 10^{14} h^{-1} M_\odot$  cluster.** The cluster is located at the top outside the figure. From top to bottom we show: **i)** the projected density field centered at the galaxy on a  $3 h^{-1} \text{Mpc}$  side box (gray background). Small colored circles correspond to individual particles inside the primordial filamentary web surrounding the galaxy at  $z = 5$  (see text for details). For reference the particles are colored according to their distance from the central galaxy at  $z = 5$ . The same set of particles (keeping their original colors) is tracked and displayed at different times, showing the disrupting and detachment of the web of filaments as the galaxy is accreted by the cluster. **ii)** Coherent structures in the dark matter velocity field after removing bulk flows above scales of  $250 h^{-1} \text{kpc}$  (see Fig. 1 for details). Matter flows from dark-blue regions and accumulates in the light-yellow structures. At early times the velocity field is highly coherent and filamentary, almost laminar streams feed the central galaxy. After the web detachment event at  $z \sim 3$  the velocity field around the galaxy becomes turbulent and the filamentary streams are lost. **iii)** Cold gas accretion rate as a function of the distance from the galaxy and divided into “cold” and “hot” modes (see text for details). The vertical dotted line shows the virial radius of the galaxy.

flecting their early evolutionary stage. Gas accretion was computed in shells of thickness  $\Delta R_{shell}$  around the center of the halo  $\mathbf{r}_h$  with velocity  $\mathbf{v}_h$  following the approach of Faucher-Giguère, Kereš & Ma (2011) as follows:

$$\dot{M} = \sum_i m_i \frac{\mathbf{v}_i - \mathbf{v}_h}{\Delta R_{shell}} \cdot \frac{\mathbf{r}_i - \mathbf{r}_h}{|\mathbf{r}_i - \mathbf{r}_h|} \quad (1)$$

where the sum is over the particles with position  $\mathbf{r}_i$ , mass  $m_i$  and velocity  $\mathbf{v}_i$  inside the shell. Gas was divided into hot and cold species by their instantaneous temperature at the threshold  $T = 10^5 \text{K}$ . The coherent and smooth velocity field provides an efficient mechanism for constant cold gas accretion producing a steady star formation. This is shown in Fig. 3 where we see a steady increase in the star formation rate from  $z = 8$  up to its peak at  $z \sim 4$ . The cold gas accre-

tion rate at  $z = 5$  is of the order of  $\sim 1 - 3 M_\odot/\text{yr}$ . Around this time the galaxy begins to interact with the proto-cluster and this is reflected in both the cold gas accretion rate and the star formation rate which shows a rapid decline. After its first interaction with the proto-cluster, the galaxy suffers several episodes of cold gas loss. Around  $z \sim 1$  the galaxy begins its accretion into the cluster. The higher density and strong tidal field associated to the cluster induces a mechanical stress in the filamentary web around the galaxy, stretching it until the point when it can no longer remain gravitationally attached (top-right panels Fig. 2). After  $z \sim 1$ , even before the galaxy has been completely accreted by the cluster, there is no recognizable filamentary web around the galaxy. The local velocity field is highly turbulent and the lack of coherent gas streams connected to the galaxy prevents the accretion of cold gas (lower panels in Fig. 2), end-

ing its efficient star formation phase. After the galaxy has been detached from its web of primordial filaments there is no mechanism that can reconnect it. From this point the galaxy can not longer accrete cold gas, depleting its internal reserves of gas and eventually stopping star formation.

### 1.5 Cosmic Web Detachment events

The star formation regulation and subsequent quenching presented in Fig. 2 is a purely mechanical/gravitational process, requiring no internal feedback from AGN. The rupture in the cold gas accretion channel is sufficient to stop star formation and, in that sense, can be considered a more fundamental process than internal feedback. Subsequent internal feedback from AGN could further prevents gas from entering the galaxy and/or cooling, removing any residual star formation (Di Matteo, Springel & Hernquist 2005; Springel et al. 2005; Best et al. 2005). Figure 2 highlights the key role of primordial filaments in the star forming history of galaxies and the decisive role of the large-scale matter distribution around a galaxy. The time when a galaxy *detaches* from its primordial filamentary web marks a tuning point in its star formation history.

The gas stripping by ram pressure and tidal interactions shown in Fig. 2 is followed by quenching but it is not the underlying process responsible for ending star formation in the satellite galaxy. The actual process that induces quenching is the removal of the feeding filaments connected to the galaxy. Without them there is no way to effective accrete cold gas to form stars and the galaxy has to rely on internal reserves. This process which we call *Cosmic Web Detachment* (CWD) is fundamentally a starvation process (Peng, Maiolino & Cochrane 2015) triggered by non-linear interactions between galaxies and other galaxies or their environment. In the following sections we describe other non-linear processes that share the same CWD mechanism to trigger star formation quenching. In the rest of this paper we use the terms CWD and web detachment interchangeably.

Figure 4 shows toy models of three basic processes that can result in CWD: i) major merger, ii) satellite accretion and iii) cosmic web infall/crossing. Note that it is possible that galaxies inside voids and walls could remain attached to their web of filaments while experiencing a reduced or even halted gas accretion due to the super Hubble expansion characteristic of under-dense regions (van de Weygaert & van Kampen 1993; Schaap 2007; Aragon-Calvo, Silk & Szalay 2011). In all cases presented in Fig. 4 the initially star-forming galaxy is connected to a web of primordial filaments from which it accretes gas. Subsequent non-linear interactions between the galaxy and a nearby structure (other galaxy, a group or a large filament/wall) detaches the galaxy from its web of feeding filaments. Following the CWD event, the galaxy can no longer accrete cold gas and star formation stops. Note that in the case of a major merger as assume that the newly merged halo could remain connected to its primordial filaments. However, these filaments are not connected to the galaxy's core. A similar situation occurs in the case of satellite accretion. After web detachment the filaments originally attached to the satellite could remain connected to the larger halo but are not able to inject gas into the satellite

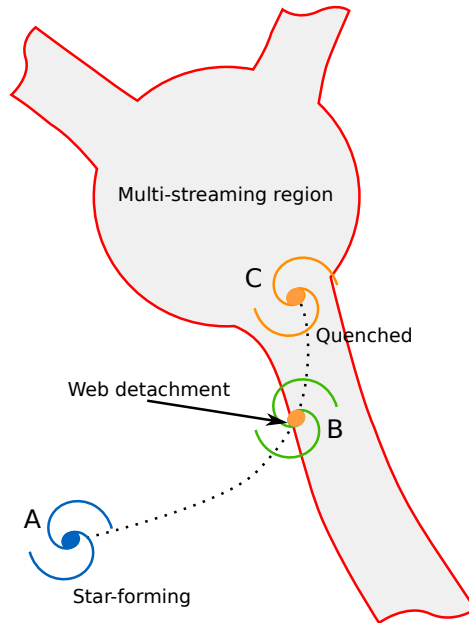


**Figure 5.** Assigning a detachment time to a galaxy. The red contour encloses regions that have been identified as multi-streaming using our Lagrangian Sheet prescription (see text for details), in this case a cluster and three large filaments connected to it. A galaxy is first detected inside a void (A) at which point it is assumed to be forming stars until it enters a multi-streaming region (B) and from this point it becomes quenched (C).

galaxy. CWD by interaction with filaments and walls may be an important quenching mechanism for dwarf galaxies (Benítez-Llambay et al. 2013).

## 2 A MULTISTREAMING FORMALISM FOR COSMIC WEB INTERACTIONS

Identifying CWD events in individual haloes is a complex and computationally expensive task that involves identifying the primordial filamentary network and following its evolution as the halo grows until the point of detachment (see Sec 1.4). This limits the practical analysis to only a few haloes with current computational resources and analysis techniques, preventing large statistical studies. We instead propose to use the dynamical state of the cosmic web to identify the most likely regions where CWD events occur. The motivation for this approximation is the idea that CWD is the result of non-linear interactions between galaxies and the cosmic web. We start by noting that in the three cases presented in Fig. 4 in order for CWD to occur the trajectories of a galaxy and a nearby structure such as another galaxy, group, filament or wall must cross. As a first approximation we can then associate web detachment events with shell-crossings at some meaningful scale. Consider for instance a major merger event (case A in Fig. 4). The two merging galaxies correspond each to an initial Lagrangian volume that collapsed and became non-linear. The merger is the union of the two Lagrangian clouds into one single Lagrangian volume. We can choose a sufficiently large smoothing scale in Lagrangian space where the patch corresponding to each of the two proto-galaxy clouds will not shell-cross



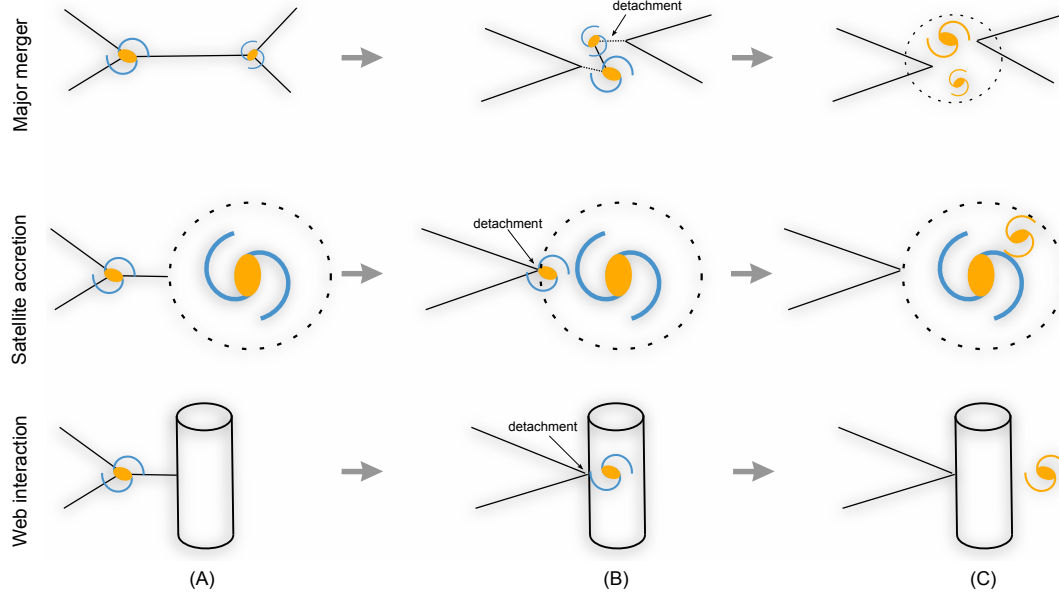


**Figure 4.** Three toy models of CWD events. From top to bottom: major merger, satellite accretion and cosmic web crossing. These events can be considered different cases of halo accretion. The basic CWD event occurs as follows: A) Initially a galaxy accretes cold gas via their web of filaments. B) The galaxy then suffers a violent detachment event from either a merger, accretion into a larger halo or accretion/crossing of a large-scale structure (here a filament).

right until the merger. At this scale the merger event will look like a shell-crossing in the smoothed Lagrangian space. The same applies to interactions between galaxies and clusters, filaments or walls.

The use of a Lagrangian smoothing to identify shell-crossing events at a scale of interests introduces the need to define such scale:

$$R_{WD} = \left( \frac{3}{4\pi\rho_m} M_{WD} \right)^{1/3}. \quad (2)$$

Where  $R_{WD}$  is the scale defining web detachment events,  $M_{WD}$  is its equivalent mass and  $\rho_m$  is the mean density of the Universe. By smoothing the initial power spectrum at this scale we produce a universe lacking structures less massive than  $M_{WD}$  (Aragon-Calvo et al. 2010; Aragon-Calvo & Szalay 2013), (see also Suhhonenko et al. 2011). We then have:

$$P_{WD}(k) = T^2(k) P_{CDM}, \quad (3)$$

where the transfer function  $T(k)$  is a filter corresponding to a spherical top-hat of radius  $R_{WD}$ . In principle we do not know the scale  $R_{WD}$ , instead of trying to derive a characteristic scale (or range of scales) we use  $R_{WD}$  corresponding to the upper halo mass threshold where star formation quenching occurs  $M_{WD} \sim 10^{12} h^{-1} M_\odot$  (Cattaneo et al. 2006; Birnboim, Dekel & Neistein 2007) as a natural scale for star formation quenching. By doing so we assume that the origin of this mass threshold is not internal processes driving quenching (which could still play an important role) but the dynamical state of the cosmic web around haloes of that mass. This gives  $R_{WD} = 2 h^{-1} \text{Mpc}$ . In contrast to the dispersion at linear scale  $\sigma_8 = 0.8$  the dispersion at the

scale of detachment is  $\sigma(R_{WD} = 2 h^{-1} \text{Mpc})_{z=0} = 1.78$  for the initial power spectrum we use.

## 2.1 Identification of multi-streaming regions

We identify CWD regions in N-body simulations as places where there has been at least one shell-crossing in the Lagrangian smoothed field and assume that haloes entering those regions undergo instantaneous CWD. Figure 5 shows a representation of a galaxy being tracked from its star forming phase to the point of web detachment and its subsequent quenched state. In practice we use the most massive progenitor line to track haloes across time (see Appendix A). In order to identify multi-streaming regions from the particle distribution we use a Lagrangian Sheet approach where the original particle distribution is used to define simplex volume elements (in 3D this corresponds to tetrahedra) (Shandarin, Habib & Heitmann 2012; Abel, Hahn & Kaehler 2012). We modify the original implementation by following Lagrangian volume elements defined by the particle's initial positions and assigning them a constant unitary density. As the simulation evolves adjacent Lagrangian volume elements in high density regions cross each other overlapping, producing *multi-streams* where more than one Lagrangian volume element occupies the same space in Eulerian coordinates (Shandarin 2011; Shandarin, Habib & Heitmann 2012; Abel, Hahn & Kaehler 2012; Ramachandra & Shandarin 2015). The complexity of the multi-streaming regions directly reflect their evolutionary stage. This idea, also exploited in the Origami cosmic web classification scheme (Neyrinck 2012; Falck, Neyrinck & Szalay 2012), (see also Falck & Neyrinck 2015), can be related to the stages of the Zel'dovich anisotropic gravitational collapse in which an initial cloud of matter collapses first into

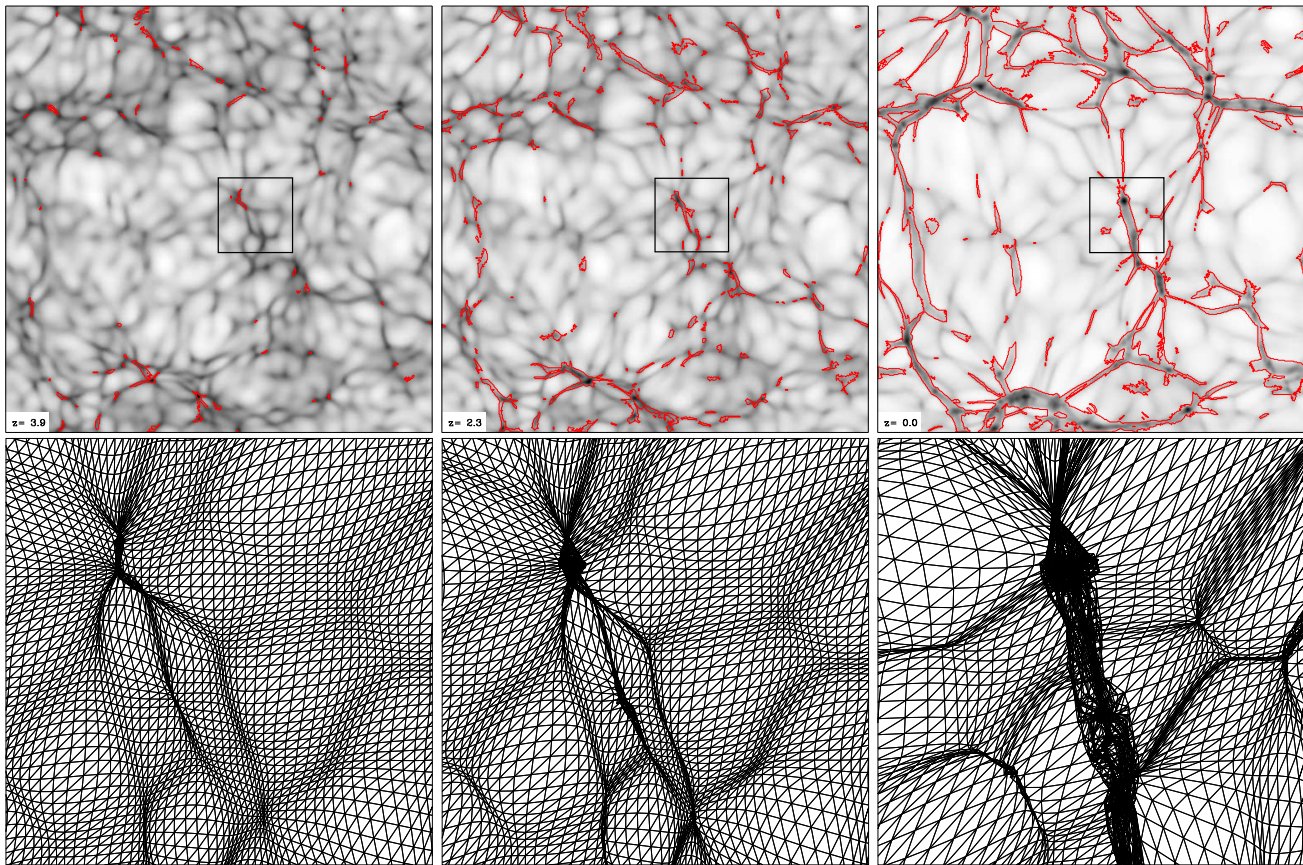


**Figure 6.** Evolution of shell-crossing regions in a  $2h^{-1}\text{Mpc}$  thick slice across the simulation box. Top panels: The gray-scale background represents the projected smoothed density field. The red contours enclose the regions where shell-crossing has occurred which correspond to CWD regions. Bottom panels: the Lagrangian tessellation used to identify multi-streaming regions inside a zoomed region (black box in top panels). For clarity we show a 2D tessellation at the (Lagrangian) center of the slice shown in the top panels. The actual computation described in the text was performed in 3D.

a two dimensional sheet, then a one-dimensional filament and finally a compact dense cluster (Zel’dovich 1970), (see also Icke 1984; Icke & van de Weygaert 1991; van de Weygaert 2002; Gurbatov, Saichev & Shandarin 2012; Hidding, Shandarin & van de Weygaert 2014).

Figure 5.1 shows the emergence of multi-streaming regions associated with CWD events at three different times. At  $z = 3.9$  tiny multi-streaming regions begin to form marking the location of large and dense peaks. At  $z = 2.3$  several multi-streaming regions have collapsed and megaparsec-scale filamentary features begin to appear. At the nodes of the multi-streaming regions we find the precursors of the large clusters seen at the present time (see Fig. B1 for a more detailed time evolution). Note the apparent lack of evolution of the CWD regions after  $z \sim 1$  in Fig. B1, reflecting the role of the cosmological constant  $\Lambda$  in the development of the cosmic web at large scales. This is also seen in Fig. 7 which shows that the rate of growth of multi-streaming regions begins to slow down around  $z \sim 2$ . We can see multi-streaming regions even inside voids although they arise at later times compared to denser environments.

By associating multi-streaming regions with CWD processes we have a convenient way of relating large-scale dynamics with small-scale halo processes such as gas accretion via primordial filaments. Compared to other approaches that

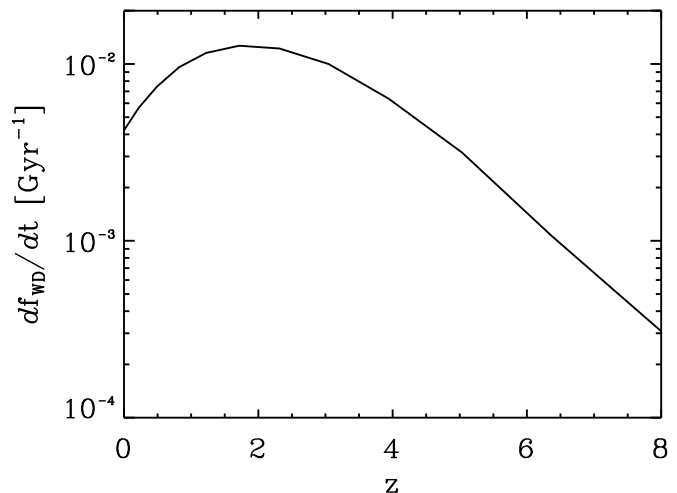


**Figure 7.** Rate of change of the fraction of volume inside multi-streaming regions as a function of time. The peak in the curve indicates the time when more volume in the cosmic web became non-linear at  $z \sim 2$ .

describe galaxies as isolated objects having environmental processes entering only indirectly (e.g. via merger trees) our



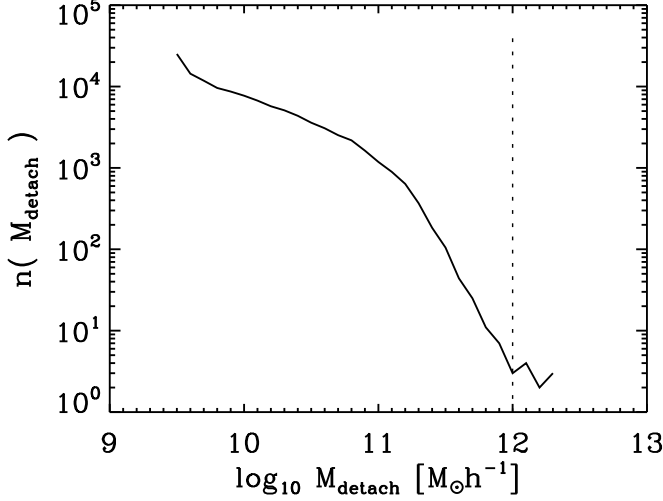


**Figure 8.** Halo mass at the time of web detachment. The dotted line indicates the upper mass-scale threshold  $M_{WD} = 10^{12}$  assumed for star formation quenching and used for the Lagrangian smoothing.

method considers cosmic environment as an integral component in galaxy evolution. This link between galaxies and their environment is the key to the ability of our multi-streaming prescription to successfully reproduce a range of environmental effects. In the rest of the paper we use the terms multi-streaming and CWD regions interchangeably.

The characteristic scale used for the Lagrangian smoothing produces, by construction, a cut in halo mass at  $M_{WD} > 10^{12} h^{-1} M_{\odot}$ . See for instance Fig. 5.1 where there are no small haloes due to the strong smoothing ( $2 h^{-1} \text{Mpc}$ ) in the initial conditions. When the Lagrangian-smoothed density field is mapped into the halo trajectories in order to identify CWD events we end up with the opposite cut in halo masses at the time of detachment. This is illustrated in Fig. 8 where we see a lack of haloes more massive than  $M_{WD}$ . Figure 8 must not be interpreted as indicating a limit in the mass of haloes in the simulation but that massive haloes ( $M > 10^{12} h^{-1} M_{\odot}$ ) being inside non-linear regions become web-detached. The distribution of halo masses in Fig. 8 has an intriguing knee at  $M \sim 10^{11} h^{-1} M_{\odot}$ . The inflection point may indicate the mass above which CWD becomes more effective which would translate to a sharp decline in star formation efficiency (Dekel & Birnboim 2006b; Behroozi, Wechsler & Conroy 2013). The knee is not directly related to the choice of the Lagrangian smoothing scale as in the case of  $M_{WD}$ . The nature and origin of the knee in the mass distribution at web detachment is worth further investigation.

### 3 MULTI-STREAMING REGIONS AND HALO HISTORY

In this section we study the history of haloes to gain insight in the type of processes occurring when a halo enters a multi-streaming region and how this could affect their star formation. The relation between halo mass accretion history and star formation is, while not completely understood yet, well established (Dekel et al.

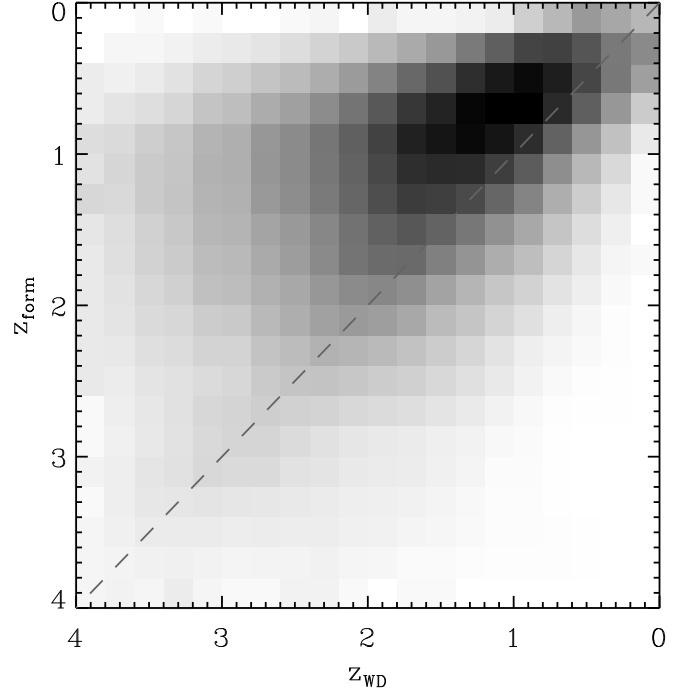


**Figure 9.** Web detachment redshift  $z_{WD}$  vs. halo formation redshift  $z_{form}$  (as a two-dimensional histogram) for haloes with mass in the range  $M > 10^{10} h^{-1} M_{\odot}$  (see text for details). The grey background indicate the counts inside each two-dimensional bin. The dashed line is shown as a reference.

2009; Mutch, Croton & Poole 2013; Watson et al. 2015; Behroozi & Silk 2015; Rodríguez-Puebla et al. 2016). The analysis we present here shows a direct link between matter accretion and the dynamical state of the local cosmic web and by doing so provides an indirect link to star formation.

#### 3.1 Formation time and Web Detachment

Figure 9 shows a comparison between web detachment redshift  $z_{WD}$  (i.e. the redshift when the halo became web-detached) and halo formation redshift  $z_{form}$  for haloes with masses  $M > 10^{10} h^{-1} M_{\odot}$ . We compute formation times following the usual definition as the time when the mass accretion history (MAH) of a halo changes its slope (Wechsler et al. 2002), usually as the result of interaction with other haloes or other elements of the cosmic web. The change in the mass accretion rate is commonly assumed to reflect some intrinsic age of the halo and hence the term formation time. However, the formation time is mostly a reflection of environmental interactions and has little to do with a halo's internal structure. We computed formation times using a two-component fit which provides a clean distinction between the two mass accretion regimes as follows:

$$M = \begin{cases} M_0 + m_1(z - z_0) & \text{if } z < z_0, \\ M_0 + m_2(z - z_0) & \text{if } z \geq z_0. \end{cases} \quad (4)$$

Where  $M_0$  and  $z_0$  are the mass accretion rate and redshift at formation time respectively, and  $m_{1,2}$  indicate the difference in the mass accretion rates. Equation 4 provides a good fit for most haloes (see Fig. ??). Halo mass loss, typical of

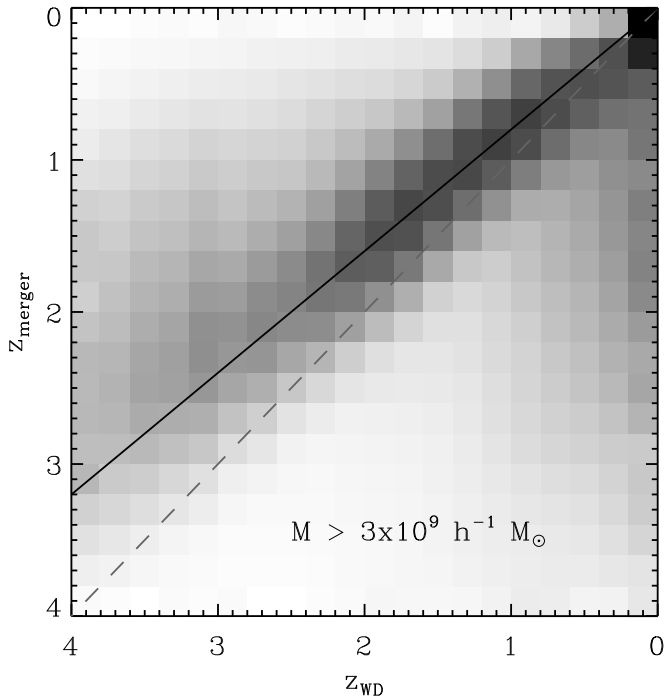


**Figure 10.** Comparison between web detachment redshift  $z_{\text{WD}}$  and the redshift of the major merger event  $z_{\text{merger}}$  (as a two-dimensional histogram). The sample is constrained to haloes that had at least one major merger event with a mass ratio between the two merging haloes of  $r_{\text{merger}} > 1.5$ . The thick black line indicating the general trend is shown as reference.

sub-haloes, is corrected by not allowing the halo’s MAH to decrease. In this approach a halo being mass-stripped will retain its mass before stripping. The formation time of the halo will usually be the time of mass stripping.

Figure 9 shows a clear correlation between  $z_{\text{WD}}$  and  $z_{\text{form}}$  with a small dispersion in redshift (which can translate to a larger dispersion in time as we approach  $z = 0$ ) in the interval  $0 < z < 2$  after which point the dispersion increases. Haloes with recent web detachment time also have a recent formation time. Haloes with an early web detachment show a less marked correlation with formation time. This may be the result of having entered multi-streaming environments at early times which could result in complex mass accretion histories that are not easily characterized by a single property such as formation time.

A key aspect of this diagram is that formation time occurs, in general, after the time of web detachment ( $z_{\text{WD}} > z_{\text{form}}$ ), in agreement with the picture of haloes first entering web-detachment regions that later affect their mass/gas accretion rates. This can be explained as galaxies can become web-detached by, for instance, entering a large filament and can in principle continue accreting mass (dark matter and baryons). If the galaxy subsequently enters a large group this will be reflected in its MAH and will produce a late formation time.

### 3.2 Major merger events

Major merger events have a significant effect in the mass accretion history of haloes. After the initial bump in mass

one can often see an immediate change in the mass accretion rate of the newly formed halo. Major mergers provide an efficient CWD mechanism by severing the primordial filaments connected to the haloes involved in the merger (see section 1.5). Therefore we should expect a close relation between major mergers and web detachment times. Figure 10 shows a comparison between the time of web detachment  $z_{\text{WD}}$  and the time of the first major merger  $z_{\text{merger}}$ . Major mergers were defined as those with a mass ratio (between the two merging haloes) of  $M_1/M_2 = 1.5$ . Only haloes with a merger ratio above this threshold were used in our analysis.

Figure 10 shows a clear correlation between web detachment events and major mergers. The correlation is even tighter than in the case of formation time (Sec. 3.1) and extends to the range  $0 < z < 2$ . Haloes tend to enter web detachment regions at earlier times than the time of their largest major merger event. This behaviour is more pronounced at high redshift ( $z < 2$ ). While the dispersion between  $z_{\text{WD}}$  and  $z_{\text{merger}}$  increases, the condition  $z_{\text{WD}} < z_{\text{merger}}$  remains valid at all times. An approximate linear fit gives  $z_{\text{merger}} \simeq 0.8 z_{\text{WD}}$ . At  $z \sim 0$  there is a small population of haloes that show no correlation between  $z_{\text{WD}}$  and  $z_{\text{merger}}$ . The origin of this small population could be purely numerical and will be investigated in future work.

## 4 SPATIAL AND TEMPORAL DISTRIBUTION OF CWD EVENTS

We now explore the spatial properties of the halo distribution segregated by CWD times. Figure 11 shows the spatial distribution of haloes that have been web-detached at early times (more than 8 Gyr ago), haloes that have undergone web detachment later (less than 0.1 Gyr ago) and one intermediate case. The CWD model gives a physical underpinning to the traditional Hubble morphological division of galaxies into “early” and “late” types. Early web-detached haloes have quenched their star formation long time ago, while late web-detached haloes are either still star forming or in the process of quenching. There is a clear trend between web detachment time and halo radius/mass. Haloes with early  $t_{\text{WD}}$  tend to be more massive and more highly clustered indicating that galaxies that entered CWD regions early mark the position of dense peaks in the initial density field (Bardeen et al. 1986). The relation between halo mass and its location inside large dense peaks naturally results in a correlation between web detachment times and spatial location. There seems to be a combination of haloes with intermediate and late web detachment times at the interior of the central void in Fig. 11, hinting a relation to the void phenomenon (Peebles 2001).

### 4.1 Clustering Properties with Web Detachment

Figure 12 gives a quantitative measure of the spatial distribution of haloes in terms of their CWD time, where the two-point correlation function of haloes is divided by different web-detachment time ranges. For our purposes we use the definition given by Hauser & Peebles (1973):

$$\xi(r) = \frac{N_d}{N_r} \frac{DD}{DR} - 1. \quad (5)$$

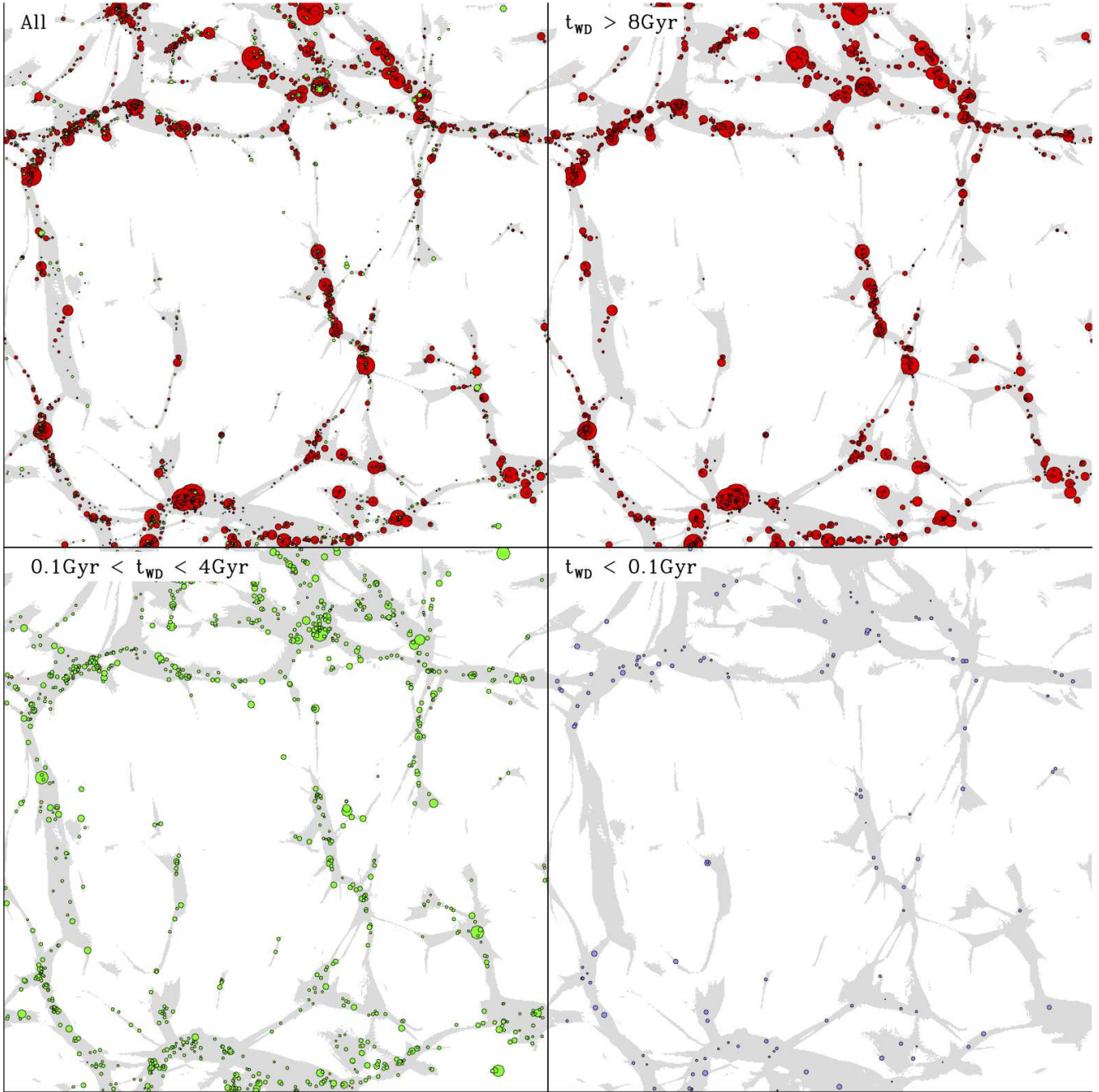


**Figure 11.** Spatial distribution of haloes divided by their web detachment time  $t_{WD}$ . The circles represent SubFind haloes scaled with their viral radius. Grey areas indicate multi-streaming regions. For clarity haloes in the bottom panels are scaled with two times their viral radius. From top-left in clockwise order: (All): Distribution of all haloes regardless of their detachment time, ( $t_{WD} > 8\text{Gyr}$ ): early-detachment with no star formation, ( $0.1\text{Gyr} < t_{WD} < 4\text{Gyr}$ ): Intermediate detachment time and ( $t_{WD} < 0.1\text{Gyr}$ ): star-forming haloes with very recent detachment. Note the strong correlation between detachment time and halo mass/radius and the different level of clustering as function of  $t_{WD}$ .

Where  $DD$  and  $DR$  are halo-halo and halo-random pair counts respectively. Figure 12 shows that early web-detached haloes have a higher degree of clustering than late web-detached haloes by almost one order of magnitude across the full range studied ( $< 10h^{-1}\text{Mpc}$ ). The effect shown in Fig. 12 is equivalent to the “assembly bias” reported by Gao, Springel & White (2005) who found that early-forming haloes are more clustered than late-forming haloes. This is

not surprising given the correlation between halo formation and web detachment times (Fig. 9). The observed change in the slope of the mass accretion history used to identify formation times often reflects non-linear interactions between haloes and their environment affecting their mass accretion.

The trend in the correlation function extends even beyond  $10h^{-1}\text{Mpc}$ . Given the simulation box size ( $64h^{-1}\text{Mpc}$ ) this should be taken with caution although the



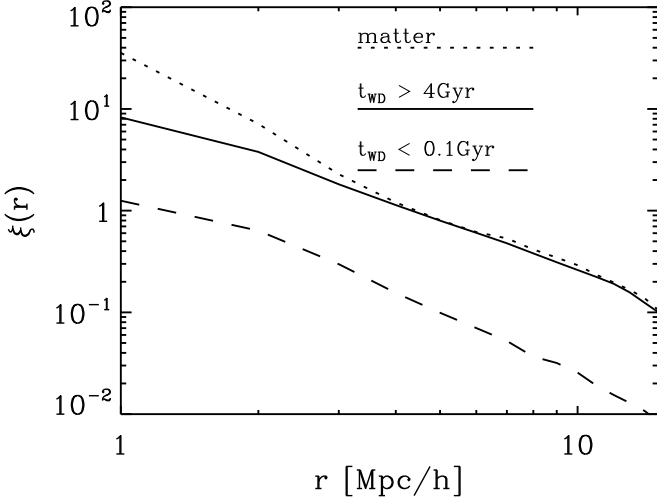


**Figure 12.** Two-point correlation function of haloes divided by early web detachment  $t_{WD} > 4\text{Gyr}$  (solid line) and late web detachment  $t_{WD} < 0.1\text{Gyr}$ . (dashed line). The dotted line shows the dark matter two-point correlation function.

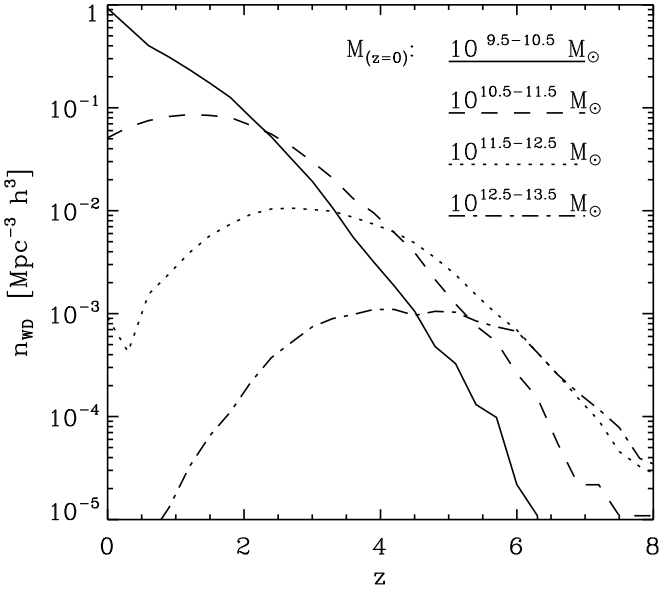


**Figure 13.** Distribution of web detachment times as function of time divided in four halo mass bins. Massive haloes get web-detached at early times while dwarf galaxies web-detach very recently. The distribution of  $t_{WD}$  for dwarf galaxies shows that they are the population that is currently undergoing CWD but has not yet reached it peak.

trend is clear. This regime corresponds to low-mass haloes that fit well with the “field” population of dwarf galaxies (Dekel & Silk 1986; Salzer 1989) which show a less pronounced correlation function compared to the enhanced massive haloes (Kaiser 1984; Politzer & Wise 1984).

#### 4.2 Anti-hierarchical CWD (downsizing)

According to the hierarchical scenario of galaxy formation small galaxies form first (and therefore their population should be composed of old stars) while massive galaxies

form later (and as such they should be forming stars at the present time). What we observe is the opposite: massive galaxies are no longer producing stars while low-mass galaxies are actively forming new stars. This apparent anti-hierarchical behavior of the star formation history of galaxies is commonly referred to as “downsizing” (Cowie et al. 1996; Heavens et al. 2004; Thomas et al. 2005; Cooper et al. 2006; Fontanot et al. 2009).

Figure 13 shows the distribution of web detachment times for several halo mass ranges (computed at the present time). There is a clear dependence between web detachment time and halo mass. The most relevant aspect of this figure is the shift in the peak from high to low redshift with decreasing halo mass. This indicates that massive haloes ( $10^{11.5-12.5} h^{-1} M_{\odot}$ ) already became web-detached at early times ( $z \sim 2$ ) while low-mass haloes ( $10^{9.5-10.5} h^{-1} M_{\odot}$ ) are still attached to their filament network or are just becoming web-detached. The peak in the web detachment time for the lowest mass bin in Fig. 13 has not been reached at the present time.

The key to downsizing is the realization that low-mass star-forming galaxies are found mostly in isolated environments and therefore their surrounding cosmic web has remained unperturbed for most of the history of the Universe. Low-mass isolated galaxies can therefore experience a slow but steady gas accretion (see Fig. 11 in Aragon-Calvo & Szalay (2013)). On the other hand, massive galaxies form in dense environments where there is a higher rate of web detachment events due to the non-linear dynamics characteristic of such environments. The net effect is the observed anti-hierarchical star formation history.

## 5 TESTING CWD WITH OBSERVATIONS

In this section we reproduce and, to some extent, explain several observations in the context of CWD. We try to use a minimum of assumptions for galaxy properties (star formation, color and quenching state) in order to emphasize the effect of CWD and we clearly indicate when we do so.

### 5.1 The cosmic star formation rate history

In order to assign star formation rates (SFR) to dark matter haloes we start by assuming a simple relation between halo mass before CWD and star formation rate. Based on the fit provided by Dekel et al. (2009) we assume an semi-linear dependence between halo mass and gas accretion/star-formation rate as:

$$SFR = A \left( \frac{M}{10^{12}} \right)^{\alpha} (1+z) \quad (6)$$

Where the constant  $A$  summarizes complex physical processes such as star formation efficiency (which in principle can also depend on halo mass and redshift). At the present time  $A$  corresponds to the SFR a halo with a mass of  $10^{12} h^{-1} M_{\odot}$  would experience if it remained connected to its network of primordial filaments (but this seems unlikely for such a massive halo) and the value of the exponent  $\alpha = 1.15$  comes from halo growth rates (Neistein, van den Bosch & Dekel 2006; Birnboim, Dekel & Neistein 2007; Neistein & Dekel

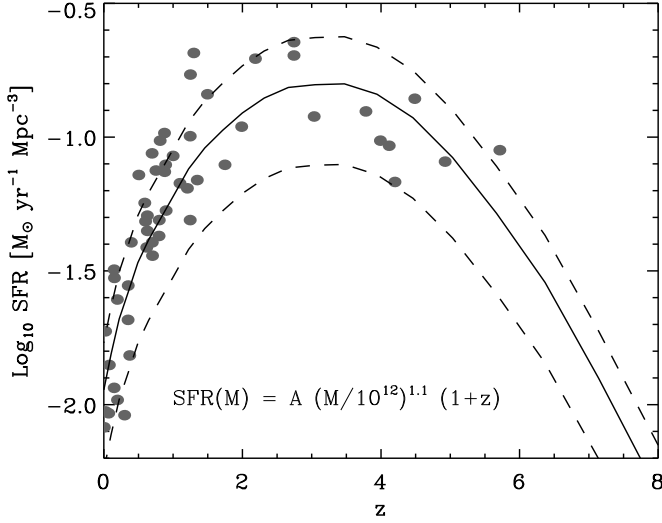


**Figure 14.** Cosmic star formation rate computed using multi-streams as proxy for web detachment and a simple model for star formation as function of halo mass (eq. 6, also shown in the figure). The three curves from top to bottom correspond to values of the constant  $A = 150, 100, 50$  respectively. The gray circles are observed data points taken from Hopkins et al. (2006) (error bars omitted for clarity).

2008; Genel et al. 2008; McBride, Fakhouri & Ma 2009; Bouché et al. 2010). We assume a SFR, given by equation 6, before CWD and an instantaneous star formation quenching after the CWD event. This behaviour is analogous to a constant star formation rate and a subsequent decline (Blanton 2006; Reddy et al. 2012; Schawinski et al. 2014). No assumptions on the morphology of the galaxy are made (although information from the merger trees could be used for this purpose).

Figure 14 shows the cosmic star formation rate history (SFRH) computed by integrating the star formation from all haloes which have not yet suffered CWD at a given redshift and assigning star formation rates as a function of halo mass following equation 6. Our CWD implementation can reproduce the general shape of the SFRH curve, in particular its peak at  $z \sim 3$  and decline to its present value more than two orders of magnitude lower (Heavens et al. 2004). The origin in the peak in the SFRH seems related to the CWD of massive haloes in the mass range  $10^{11.5-12.5} h^{-1} M_{\odot}$  with a peak at around  $z \sim 2 - 3$  (Fig. 13) indicating the time when the rate of web detachment was maximum (Fig. 7).

The peak in the SFR at  $z \sim 2$  corresponds to just 3.2 Gyr after the Big Bang. At this point the megaparsec-scale structures in the cosmic web are still in development (see Figs. and ) and will not reach its present-time large-scale features until  $z \sim 1$ . Figure 7 shows the rate of change of the fraction of volume inside multi-streaming regions as a function of time. The close relation between the rate at which regions in the Universe become non-linear, web-detachment times and the peak in the cosmic star formation rate suggests a causal link between these processes. If that is the case then the properties of galaxies, and in particular their star formation history, could be a reflection of the dynamical state of their surrounding cosmic web.

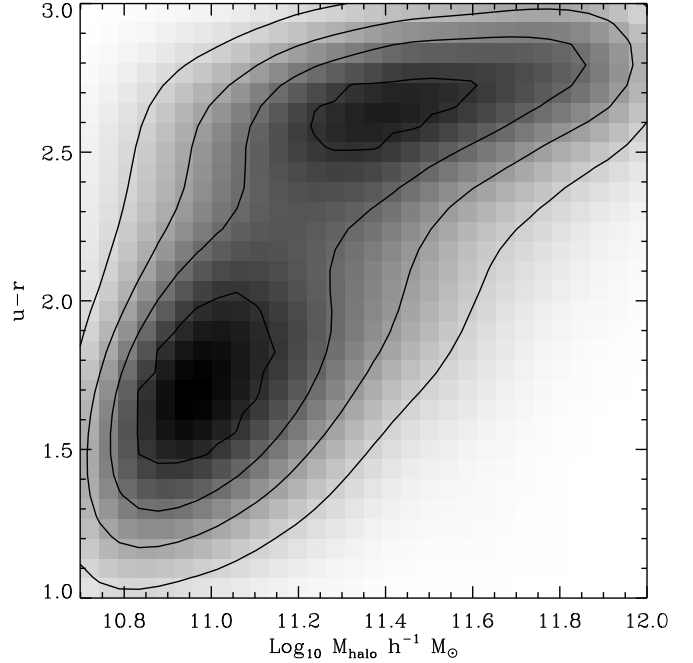


**Figure 15.** Galaxy color bimodality in the mass-color diagram. The grey background corresponds to the two-dimensional mass-color distribution. We show three contours to highlight the shape of the two regions. The distribution was smoothed for clarity.

## 5.2 The bimodality in the color distribution of galaxies

Figure 15 shows the distribution of galaxy colors with halo mass. Galaxy colors were assigned from a template of galaxies selected from the Sloan Digital Sky Survey (see Appendix B2 for details on the database query). Dark matter haloes in our simulation were *matched* to galaxies in the template by assuming a monotonic relation between web detachment time  $t_{WD}$  and galaxy color in a similar way as done by Hearin & Watson (2013). By doing so we assume that galaxies that have an early CWD time have an older stellar population and are redder than galaxies with a later CWD time. The matching was done by sorting haloes (more massive than  $5 \times 10^{10} h^{-1} M_{\odot}$ ) by their  $t_{WD}$  and also sorting SDSS galaxies by their  $u - r$  color. The two regions in the mass-color diagram arise by the mapping of halo masses and web-detachment at different times. The mass-color distribution in Fig. 15 shows a clear bimodal distribution with the blue cloud corresponding to late-detachment haloes and a red cloud of early web detachment haloes. The ability of our CWD implementation to reproduce the mass-color diagram comes not from the bimodality in color (intrinsic to the SDSS galaxy sample), but from the halo mass distribution, which depends on the distribution of  $t_{WD}$  (see Fig. 13).

It is not straightforward to interpret the green valley population in Fig. 15 in the context of CWD since the color distribution of the SDSS galaxies is intrinsically bimodal. Constraining the green valley to a horizontal band in the color-mass diagram implies independence of color with halo mass/luminosity in contrast to quenching models based on a halo mass threshold (Cattaneo et al. 2006; Birnboim, Dekel & Neistein 2007; Dekel et al. 2009) although the narrow range in mass corresponding to the

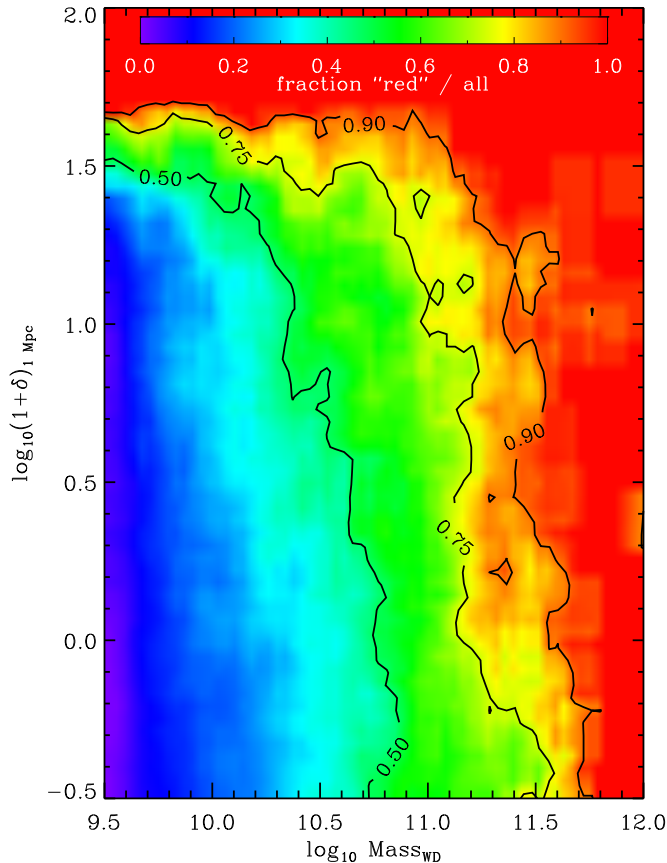


**Figure 16.** Fraction of red galaxies with respect to the total population as a function of halo mass at the time of detachment and local density (see text for details).

green valley makes this unclear. If cosmic web detachment is one of the possible paths for a galaxy through the green valley then this corresponds to galaxies with  $t_{WD} \sim 8.5$  Gyr. However, green valley galaxies are most likely a composite population of galaxies in the process of quenching and already quenched galaxies that are undergoing a new star forming phase.

### 5.3 Star formation as function of mass and density

Figure 16 shows the fraction of red galaxies (here defined as galaxies with  $t_{WD} > 10$  Gyr) as a function of halo mass and local density. This plot is based on Fig. 6 in Peng et al. (2010) where they analyzed a sample of galaxies from the SDSS. The local density was computed using a top-hat window of radius  $r = 1h^{-1}$  Mpc centered on each halo and counting the dark matter particles inside the window. This is in principle different than computing densities from the (biased) galaxy population but for purposes of comparison it is adequate. Surprisingly our simple implementation of CWD reproduces to a great degree the relation between fraction of red galaxies, their mass and density. For a given halo mass the fraction of red galaxies in low-density environments is lower than for dense environments and for a given density the fraction increases with halo mass. This is interpreted by Peng et al. (2010) as suggesting two separate mechanisms

of "environmental quenching" and "mass quenching". However, this relation must be taken with caution since halo mass and density are correlated (see Fig. B3) so the interpretation of two different processes is not straightforward. In the CWD framework we interpret the increase in density with an increase in the environment's complexity leading to CWD events and quenching. On the other hand, we expect massive haloes to populate dense environments so the increase in the red fraction with mass could also be interpreted as a consequence of the increase in density.

The CWD framework also provides a simple explanation for the lack of quenched dwarf population in voids (Geha et al. 2012). Figure 16 shows that the fraction of web-detached haloes, compared to the general population, is the lowest for dwarf haloes in low density environments. Dwarf galaxies in the low-dense field (i.e. voids and walls) remain connected to their network of filaments. This is seen in our multi-streaming formalism as haloes that have not entered yet into non-linear multi-streaming regions. We should expect to find star-forming dwarf galaxies at the present time in voids and walls.

## 6 DISCUSSION

### 6.1 CWD, cosmic SFR and AGN causal links

The peak in the AGN redshift distribution around  $z \sim 2$  (Shaver et al. 1996; Page et al. 2001; Hasinger, Miyaji & Schmidt 2005) is tantalizingly similar to the peak in the density of web detachment for haloes in the mass range  $\sim 10^{11.5-12.5} h^{-1} M_{\odot}$  (Fig. 13), the peak in the rate of change in the fraction of regions becoming non-linear (Fig. 7) and the peak in the star formation rate (Fig. 14). If we assume a link between AGN and CWD events then the anti-hierarchical behaviour seen in the time distribution of CWD events with mass (Fig. 13) could explain the difference in the peak in AGN with luminosities cited as AGN downsizing (Hasinger, Miyaji & Schmidt 2005; Babić et al. 2007; Enoki et al. 2014). While this coincidence alone is not enough to establish a causal link it suggests a relation between these processes.

### 6.2 Can CWD trigger AGN?

The process responsible of injecting gas into the central black hole of a galaxy hosting an AGN is still not well understood. One proposed mechanism is bar instability which may induce angular momentum loss. Major mergers and strong tidal interactions provide a clear mechanism for angular momentum loss, although there is strong evidence that they are responsible only for the most luminous AGN (Treister et al. 2012; Chiaberge et al. 2015). One process not previously considered as a trigger for AGN is the interaction between galaxies and the cosmic web i.e. walls, filaments and clusters. As a galaxy is accreted by a cosmic web element its network of filaments will be detached. However, at the same time the galaxy will experience an increase in gas pressure along the direction of the accretion, as seen in galaxy mergers (Barnes & Hernquist 1991; Mihos & Hernquist 1994a,b; Hopkins et al. 2006; Silverman et al. 2009; Knapen & Cisternas 2015). A galaxy



entering a wall, filament of cluster is effectively being slammed against a wall of gas (Benítez-Llambay et al. 2013). This may provide just the right amount of perturbation to inject gas into the central black hole and activate the AGN. Galaxy-LSS interactions may also provide a perturbation mechanism to trigger the formation of bars and even disk warping (Arsenault 1989; Moles, Marquez & Perez 1995; Knapen 2005; Hao et al. 2009; Oh, Oh & Yi 2012; Lee et al. 2012). This would explain observed correlations between AGN activity, bars and star formation quenching, providing the causal link between these related processes.

### 6.3 Searching for primordial filaments in voids and walls, the case of the Milky Way

One aspect of CWD worth exploring is its relation with the different elements of the cosmic web. In particular galaxies in voids and walls, given their relatively dynamically young environment, could still be connected to their web of primordial filaments and thus be star forming (Ceccarelli, Padilla & Lambas 2008; Liu et al. 2015; Moorman et al. 2016). The super-Hubble expansion in such environments (see Sec. 1.5) acts like a regulator for gas accretion resulting in a slow and steady star formation (Aragon-Calvo, Silk & Szalay 2011; Ricciardelli et al. 2014; Das et al. 2015). Present-time voids, and to a lesser extent walls, are ideal environments to search for primordial filaments. Recent deep observations have already found examples of thin filaments connected to void galaxies (Kreckel et al. 2012; Beygu et al. 2013; Alpaslan et al. 2014).

Our own Milk Way may have evidence for gas supply from cosmological origin, which we assume to be driven by primordial filaments in the plane of the Local Sheet. The Milky Way galaxy is located near the center of a large cosmological wall with two large voids on each side (Tully & Fisher 1987; Tully et al. 2008) and is currently forming  $\sim 1 \text{ h}^{-1} \text{ M}_{\odot}$  per year. At this rate the gas reserves in the Milky Way would deplete within a timescale shorter than Hubble time (Noeske et al. 2007; Salim et al. 2007) but what we observe is a relatively constant star formation rate and Deuterium abundance in the solar neighborhood in the last several Gyr (Binney, Dehnen & Bertelli 2000). The low SFR of the MW, given its mass, could be due to super-Hubble regulation or perhaps interactions with the Local Sheet which may have affected its feeding filaments. Another example of a galaxy with possible cosmological gas accretion is NGC 6946, the “Fireworks galaxy” featuring a high supernovae rate (9 per century) and a possible detection of filamentary structures (Pisano 2014). Based on the CWD model we can predict that most galaxies with a long and steady star formation history which are forming stars at the present time should be found in voids and walls.

### 6.4 The origin of red spirals

Not all CWD events are the result of violent gravitational interactions. When a galaxy is accreted by a large filament or cluster but without experiencing major mergers this can result in CWD without morphological change. Good candidates for this scenario are the red spirals seen in dense environments

(Couch et al. 1998; Dressler et al. 1999; Poggianti et al. 1999; Masters et al. 2010; Bekki, Couch & Shioya 2002) and SO (Larson, Tinsley & Caldwell 1980). This is consistent with findings that satellites are affected more in color than morphology (van den Bosch et al. 2008).

## 7 CONCLUSIONS

The CWD model presented here provides a simple mechanism to stop star formation in galaxies by separating a galaxy from its main star-forming gas supply. CWD is to first order purely mechanical/gravitational. The nature of the particular CWD event determines the fate of the remaining gas inside the galaxy: major mergers will result in most of the gas being consumed in a starburst, often followed by a change in the galaxy’s morphology, while less violent detachments will allow gas reservoirs to be slowly consumed until depleted within a few Gyr (Bauermeister, Blitz & Ma 2010). Star formation histories of high redshift galaxies support the picture of gas accretion→star formation (web attached), starburst (web detaching) and instantaneous or slow decline (web detached) (Reddy et al. 2012; Blanton 2006). Schawinski et al. (2014) found evidence that galaxies spiral galaxies move through the green valley when their external gas supply ends but continue to burn their remaining gas into stars. Ellipticals on the other hand require an scenario where both the accreting gas and their reservoirs are consumed in a very short time scale.

Gas strangulation and quenching are two distinct ways of reducing the SFR. Quenching is in principle instantaneous, although in practice it is inefficient. Strangulation cuts the gas supply and allow star formation to continue at a decreasing rate. Evidence has been found for bimodality in the metallicity stellar mass relation between passive and star-forming galaxies that points to both processes in action for ETGs. Strangulation applies to galaxies below  $\sim 10^{11} \text{ h}^{-1} \text{ M}_{\odot}$ , These galaxies continue to grow in stellar mass and metallicity for some 4 billion years after the gas supply terminates, which we interpret here as due to web detachment.

CWD is a strangulation process. We have shown that it fits the data on SFR histories, the mass color bimodality and environmental dependence of red galaxy fraction. We therefore propose that it is an effective and natural implementation of strangulation. Indeed, AGNs are not needed to drive outflows in our approach, even for massive galaxies. Web detachment naturally regulates the gas supply at all masses. Of course AGNs may well be a consequence both of mass and of gas accretion as well as of mergers, and almost certainly play a role in quenching massive galaxies, above  $\sim 10^{11} \text{ h}^{-1} \text{ M}_{\odot}$ .

## 8 ACKNOWLEDGEMENTS

MA would like to thank the many colleagues with whom he discussed, over the course of several years, aspects of the work presented here, in particular Joel Primack, Bernard Jones, Rien van de Weygaert, Alex Szalay and Jaan Einasto. MA is grateful for support from the Gordon and Betty Moore foundation while at JHU, where this work originated,

and a Big Data seed grant from the office for Research and Economic Development, UC Riverside. This work has been carried out in part at IAP under the ILP LABEX (ANR-10-LABX-63) supported by French state funds managed by the ANR within the Investissements d'Avenir programme under reference ANR-11-IDEX-0004-02. The work of MN and JS was supported by ERC Project No. 267117 (DARK) hosted by Université Pierre et Marie Curie (UPMC) - Paris 6, PI J. Silk. JS acknowledges the support of the JHU by NSF grant OIA-1124403. The authors would like to thank Volker Springel for making his code Gadget-3 available.

The SDSS is managed by the Astrophysical Research Consortium for the Participating Institutions. The Participating Institutions are the American Museum of Natural History, Astrophysical Institute Potsdam, University of Basel, University of Cambridge, Case Western Reserve University, University of Chicago, Drexel University, Fermilab, the Institute for Advanced Study, the Japan Participation Group, Johns Hopkins University, the Joint Institute for Nuclear Astrophysics, the Kavli Institute for Particle Astrophysics and Cosmology, the Korean Scientist Group, the Chinese Academy of Sciences (LAMOST), Los Alamos National Laboratory, the Max-Planck-Institute for Astronomy (MPIA), the Max-Planck-Institute for Astrophysics (MPA), New Mexico State University, Ohio State University, University of Pittsburgh, University of Portsmouth, Princeton University, the United States Naval Observatory, and the University of Washington.

## REFERENCES

- Abadi M. G., Moore B., Bower R. G., 1999, *MNRAS*, 308, 947
- Abazajian K. N. et al., 2009, *ApJS*, 182, 543
- Abel T., Hahn O., Kaehler R., 2012, *MNRAS*, 427, 61
- Alpaslan M. et al., 2016, *MNRAS*, 457, 2287
- Alpaslan M. et al., 2014, *MNRAS*, 440, L106
- Aragon-Calvo M. A., 2012, *ArXiv e-prints*
- Aragón-Calvo M. A., Jones B. J. T., van de Weygaert R., van der Hulst J. M., 2007a, *A&A*, 474, 315
- Aragon-Calvo M. A., Neyrinck M. C., Silk J., 2014, *ArXiv e-prints*
- Aragon-Calvo M. A., Silk J., Szalay A. S., 2011, *MNRAS*, 415, L16
- Aragon-Calvo M. A., Szalay A. S., 2013, *MNRAS*, 428, 3409
- Aragon-Calvo M. A., van de Weygaert R., Araya-Melo P. A., Platen E., Szalay A. S., 2010, *MNRAS*, 404, L89
- Aragón-Calvo M. A., van de Weygaert R., Jones B. J. T., 2010, *MNRAS*, 408, 2163
- Aragón-Calvo M. A., van de Weygaert R., Jones B. J. T., van der Hulst J. M., 2007b, *ApJLett*, 655, L5
- Aragon-Calvo M. A., Yang L. F., 2014, *MNRAS*, 440, L46
- Arsenault R., 1989, *A&A*, 217, 66
- Babić A., Miller L., Jarvis M. J., Turner T. J., Alexander D. M., Croom S. M., 2007, *A&A*, 474, 755
- Baldry I. K., Glazebrook K., Brinkmann J., Ivezić Ž., Lupton R. H., Nichol R. C., Szalay A. S., 2004, *ApJ*, 600, 681
- Balsara D., Livio M., O'Dea C. P., 1994, *ApJ*, 437, 83
- Bardeen J. M., Bond J. R., Kaiser N., Szalay A. S., 1986, *ApJ*, 304, 15
- Barnes J., Hut P., 1986, *Nature*, 324, 446
- Barnes J. E., Hernquist L. E., 1991, *ApJLett*, 370, L65
- Bauermeister A., Blitz L., Ma C.-P., 2010, *ApJ*, 717, 323
- Behroozi P. S., Silk J., 2015, *ApJ*, 799, 32
- Behroozi P. S., Wechsler R. H., Conroy C., 2013, *ApJLett*, 762, L31
- Bekki K., Couch W. J., Shioya Y., 2002, *ApJ*, 577, 651
- Bell E. F. et al., 2004, *ApJ*, 608, 752
- Benítez-Llambay A., Navarro J. F., Abadi M. G., Gottlöber S., Yepes G., Hoffman Y., Steinmetz M., 2013, *ApJLett*, 763, L41
- Benson A. J., Lacey C. G., Baugh C. M., Cole S., Frenk C. S., 2002, *MNRAS*, 333, 156
- Benson A. J., Pearce F. R., Frenk C. S., Baugh C. M., Jenkins A., 2001, *MNRAS*, 320, 261
- Best P. N., Kauffmann G., Heckman T. M., Brinchmann J., Charlot S., Ivezić Ž., White S. D. M., 2005, *MNRAS*, 362, 25
- Beygu B., Kreckel K., van de Weygaert R., van der Hulst J. M., van Gorkom J. H., 2013, *A&A*, 445, 120
- Binney J., Dehnen W., Bertelli G., 2000, *MNRAS*, 318, 658
- Birnboim Y., Dekel A., Neistein E., 2007, *MNRAS*, 380, 339
- Blanton M. R., 2006, *ApJ*, 648, 268
- Blanton M. R., Eisenstein D., Hogg D. W., Schlegel D. J., Brinkmann J., 2005, *ApJ*, 629, 143
- Bond J. R., Kofman L., Pogossyan D., 1996, *Nature*, 380, 603
- Boselli A., Boissier S., Cortese L., Gavazzi G., 2008, *ApJ*, 674, 742
- Bouché N. et al., 2010, *ApJ*, 718, 1001
- Cattaneo A., Dekel A., Devriendt J., Guiderdoni B., Blaizot J., 2006, *MNRAS*, 370, 1651
- Ceccarelli L., Padilla N., Lambas D. G., 2008, *MNRAS*, 390, L9
- Chen Y.-C. et al., 2015, *ArXiv e-prints*
- Chiaberge M., Gilli R., Lotz J. M., Norman C., 2015, *ApJ*, 806, 147
- Coil A. L. et al., 2008, *ApJ*, 672, 153
- Cole S., 1991, *ApJ*, 367, 45
- Cole S., Lacey C. G., Baugh C. M., Frenk C. S., 2000, *MNRAS*, 319, 168
- Conroy C., Wechsler R. H., Kravtsov A. V., 2006, *ApJ*, 647, 201
- Cooper M. C. et al., 2007, *MNRAS*, 376, 1445
- Cooper M. C. et al., 2006, *MNRAS*, 370, 198
- Couch W. J., Barger A. J., Smail I., Ellis R. S., Sharples R. M., 1998, *ApJ*, 497, 188
- Cowie L. L., Songaila A., Hu E. M., Cohen J. G., 1996, *A&A*, 112, 839
- Danovich M., Dekel A., Hahn O., Teyssier R., 2012, *MNRAS*, 422, 1732
- Darvish B., Mobasher B., Sobral D., Rettura A., Scoville N., Faisst A., Capak P., 2016, *ApJ*, 825, 113
- Darvish B., Sobral D., Mobasher B., Scoville N. Z., Best P., Sales L. V., Smail I., 2014, *ApJ*, 796, 51
- Das M., Saito T., Iono D., Honey M., Ramya S., 2015, *ApJ*, 815, 40
- Davis M., Efstathiou G., Frenk C. S., White S. D. M., 1985, *ApJ*, 292, 371

- De Rijcke S., Van Hese E., Buyle P., 2010, *ApJLett*, 724, L171
- Dekel A., Birnboim Y., 2006a, *MNRAS*, 368, 2
- Dekel A., Birnboim Y., 2006b, *MNRAS*, 368, 2
- Dekel A. et al., 2009, *Nature*, 457, 451
- Dekel A., Silk J., 1986, *ApJ*, 303, 39
- Di Matteo T., Springel V., Hernquist L., 2005, *Nature*, 433, 604
- Dressler A., 1980, *ApJ*, 236, 351
- Dressler A., Smail I., Poggianti B. M., Butcher H., Couch W. J., Ellis R. S., Oemler, Jr. A., 1999, *ApJSupp*, 122, 51
- Einasto J. et al., 2011, *A&A*, 534, A128
- Enoki M., Ishiyama T., Kobayashi M. A. R., Nagashima M., 2014, *ApJ*, 794, 69
- Faber S. M. et al., 2007, *ApJ*, 665, 265
- Falck B., Neyrinck M. C., 2015, *MNRAS*, 450, 3239
- Falck B. L., Neyrinck M. C., Szalay A. S., 2012, *ApJ*, 754, 126
- Faucher-Giguère C.-A., Kereš D., 2011, *MNRAS*, 412, L118
- Faucher-Giguère C.-A., Kereš D., Ma C.-P., 2011, *MNRAS*, 417, 2982
- Feldmann R., Mayer L., 2015, *MNRAS*, 446, 1939
- Fontanot F., De Lucia G., Monaco P., Somerville R. S., Santini P., 2009, *MNRAS*, 397, 1776
- Fujita Y., 2004, *PASJ*, 56, 29
- Gao L., Springel V., White S. D. M., 2005, *MNRAS*, 363, L66
- Geha M., Blanton M. R., Yan R., Tinker J. L., 2012, *ApJ*, 757, 85
- Geller M. J., Huchra J. P., 1989, *Science*, 246, 897
- Genel S. et al., 2008, *ApJ*, 688, 789
- Goto T. et al., 2003, *PASJ*, 55, 739
- Gottlöber S., Lokas E. L., Klypin A., Hoffman Y., 2003, *MNRAS*, 344, 715
- Gunn J. E., Gott, III J. R., 1972, *ApJ*, 176, 1
- Gurbatov S. N., Saichev A. I., Shandarin S. F., 2012, *Physics Uspekhi*, 55, 223
- Hahn O., Carollo C. M., Porciani C., Dekel A., 2007, *MNRAS*, 381, 41
- Hao L., Jogee S., Barazza F. D., Marinova I., Shen J., 2009, in *Astronomical Society of the Pacific Conference Series*, Vol. 419, *Galaxy Evolution: Emerging Insights and Future Challenges*, Jogee S., Marinova I., Hao L., Blanc G. A., eds., p. 402
- Harford G. A., Hamilton A. J. S., 2016, *ArXiv e-prints*
- Hasinger G., Miyaji T., Schmidt M., 2005, *A&A*, 441, 417
- Hatton S., Devriendt J. E. G., Ninin S., Bouchet F. R., Guiderdoni B., Vibert D., 2003, *MNRAS*, 343, 75
- Hauser M. G., Peebles P. J. E., 1973, *ApJ*, 185, 757
- Hearin A. P., Watson D. F., 2013, *MNRAS*, 435, 1313
- Hearin A. P., Watson D. F., Becker M. R., Reyes R., Berlind A. A., Zentner A. R., 2014, *MNRAS*, 444, 729
- Heavens A., Panter B., Jimenez R., Dunlop J., 2004, *Nature*, 428, 625
- Hester J. A., 2006, *ApJ*, 647, 910
- Hidding J., Shandarin S. F., van de Weygaert R., 2014, *MNRAS*, 437, 3442
- Hockney R. W., Eastwood J. W., 1988, *Computer simulation using particles*
- Hogg D. W. et al., 2004, *ApJLett*, 601, L29
- Hogg D. W. et al., 2003, *ApJLett*, 585, L5
- Hopkins P. F., Hernquist L., Cox T. J., Di Matteo T., Robertson B., Springel V., 2006, *ApJSupp*, 163, 1
- Icke V., 1984, *MNRAS*, 206, 1P
- Icke V., van de Weygaert R., 1991, *QJRAS*, 32, 85
- Jahnke K., Macciò A. V., 2011, *ApJ*, 734, 92
- Joeveer M., Einasto J., 1978, in *IAU Symposium*, Vol. 79, *Large Scale Structures in the Universe*, Longair M. S., Einasto J., eds., pp. 241–250
- Kaiser N., 1984, *ApJLett*, 284, L9
- Kauffmann G., Li C., Zhang W., Weinmann S., 2013, *MNRAS*, 430, 1447
- Kauffmann G., White S. D. M., Guiderdoni B., 1993, *MNRAS*, 264, 201
- Kawata D., Mulchaey J. S., 2008, *ApJLett*, 672, L103
- Kereš D., Katz N., Weinberg D. H., Davé R., 2005, *MNRAS*, 363, 2
- Klypin A. A., Shandarin S. F., 1983, *MNRAS*, 204, 891
- Knapen J. H., 2005, in *American Institute of Physics Conference Series*, Vol. 783, *The Evolution of Starbursts*, Hüttmeister S., Manthey E., Bomans D., Weis K., eds., pp. 171–181
- Knapen J. H., Cisternas M., 2015, *ApJLett*, 807, L16
- Kodama T., Bower R. G., 2001, *MNRAS*, 321, 18
- Kreckel K., Platen E., Aragón-Calvo M. A., van Gorkom J. H., van de Weygaert R., van der Hulst J. M., Beygu B., 2012, *A&A*, 544, 16
- Kronberger T., Kapferer W., Unterguggenberger S., Schindler S., Ziegler B. L., 2008, *A&A*, 483, 783
- Lacey C., Silk J., 1991, *ApJ*, 381, 14
- Larson R. B., Tinsley B. M., Caldwell C. N., 1980, *ApJ*, 237, 692
- Lee G.-H., Woo J.-H., Lee M. G., Hwang H. S., Lee J. C., Sohn J., Lee J. H., 2012, *ApJ*, 750, 141
- Liu C.-X., Pan D. C., Hao L., Hoyle F., Constantin A., Vogeley M. S., 2015, *ApJ*, 810, 165
- Lucy L. B., 1977, *A&A*, 82, 1013
- Masters K. L. et al., 2010, *MNRAS*, 405, 783
- Mayer L., Mastropietro C., Wadsley J., Stadel J., Moore B., 2006, *MNRAS*, 369, 1021
- McBride J., Fakhouri O., Ma C.-P., 2009, *MNRAS*, 398, 1858
- McCarthy I. G., Frenk C. S., Font A. S., Lacey C. G., Bower R. G., Mitchell N. L., Balogh M. L., Theuns T., 2008, *MNRAS*, 383, 593
- Mihos J. C., Hernquist L., 1994a, *ApJLett*, 425, L13
- Mihos J. C., Hernquist L., 1994b, *ApJLett*, 431, L9
- Moles M., Marquez I., Perez E., 1995, *ApJ*, 438, 604
- Monaco P., Fontanot F., Taffoni G., 2007, *MNRAS*, 375, 1189
- Moore B., Katz N., Lake G., Dressler A., Oemler A., 1996, *Nature*, 379, 613
- Moore B., Lake G., Katz N., 1998, *ApJ*, 495, 139
- Moorman C. M., Moreno J., White A., Vogeley M. S., Hoyle F., Giovanelli R., Haynes M. P., 2016, *ArXiv e-prints*
- Mori M., Burkert A., 2000, *ApJ*, 538, 559
- Mutch S. J., Croton D. J., Poole G. B., 2013, *MNRAS*, 435, 2445
- Navarro J. F., Abadi M. G., Steinmetz M., 2004, *ApJLett*, 613, L41
- Neistein E., Dekel A., 2008, *MNRAS*, 388, 1792
- Neistein E., van den Bosch F. C., Dekel A., 2006, *MNRAS*, 372, 933



Neyrinck M. C., 2012, MNRAS, 427, 494  
 Noeske K. G. et al., 2007, ApJLett, 660, L47  
 Oh S., Oh K., Yi S. K., 2012, ApJSupp, 198, 4  
 Onions J. et al., 2012, MNRAS, 423, 1200  
 Page M. J., Stevens J. A., Mittaz J. P. D., Carrera F. J., 2001, Science, 294, 2516  
 Park D., Lee J., 2009, MNRAS, 397, 2163  
 Peebles P. J. E., 2001, ApJ, 557, 495  
 Peng C. Y., 2007, ApJ, 671, 1098  
 Peng Y., Maiolino R., Cochrane R., 2015, Nature, 521, 192  
 Peng Y.-j. et al., 2010, ApJ, 721, 193  
 Pisano D. J., 2014, A&A, 147, 48  
 Planck Collaboration et al., 2015, ArXiv e-prints  
 Poggianti B. M., Smail I., Dressler A., Couch W. J., Barger A. J., Butcher H., Ellis R. S., Oemler, Jr. A., 1999, ApJ, 518, 576  
 Politzer H. D., Wise M. B., 1984, ApJLett, 285, L1  
 Quilis V., Moore B., Bower R., 2000, Science, 288, 1617  
 Ramachandra N. S., Shandarin S. F., 2015, MNRAS, 452, 1643  
 Reddy N. A., Pettini M., Steidel C. C., Shapley A. E., Erb D. K., Law D. R., 2012, ApJ, 754, 25  
 Rees M. J., Ostriker J. P., 1977, MNRAS, 179, 541  
 Ricciardelli E., Cava A., Varela J., Quilis V., 2014, MNRAS, 445, 4045  
 Rieder S., van de Weygaert R., Cautun M., Beygu B., Portegies Zwart S., 2013, MNRAS, 435, 222  
 Rodríguez-Puebla A., Primack J. R., Behroozi P., Faber S. M., 2016, MNRAS, 455, 2592  
 Salim S. et al., 2007, ApJSupp, 173, 267  
 Salzer J. J., 1989, ApJ, 347, 152  
 Schaap W. E., 2007, PhD thesis, Kapteyn Astronomical Institute  
 Schaap W. E., van de Weygaert R., 2000, A&A, 363, L29  
 Schawinski K. et al., 2014, MNRAS, 440, 889  
 Schiminovich D. et al., 2007, ApJSupp, 173, 315  
 Shandarin S., Habib S., Heitmann K., 2012, Phys. Rev. D, 85, 083005  
 Shandarin S. F., 2011, JCAP, 5, 015  
 Shaver P. A., Wall J. V., Kellermann K. I., Jackson C. A., Hawkins M. R. S., 1996, Nature, 384, 439  
 Sheth R. K., van de Weygaert R., 2004, MNRAS, 350, 517  
 Silk J., Rees M. J., 1998, A&A, 331, L1  
 Silverman J. D. et al., 2009, ApJ, 696, 396  
 Somerville R. S., Hopkins P. F., Cox T. J., Robertson B. E., Hernquist L., 2008, MNRAS, 391, 481  
 Somerville R. S., Primack J. R., 1999, MNRAS, 310, 1087  
 Springel V., Hernquist L., 2002, MNRAS, 333, 649  
 Springel V., Hernquist L., 2003, MNRAS, 339, 312  
 Springel V. et al., 2005, Nature, 435, 629  
 Strateva I. et al., 2001, A&A, 122, 1861  
 Suhhonenko I. et al., 2011, A&A, 531, A149  
 Thomas D., Maraston C., Bender R., Mendes de Oliveira C., 2005, ApJ, 621, 673  
 Treister E., Schawinski K., Urry C. M., Simmons B. D., 2012, ApJLett, 758, L39  
 Treu T., Ellis R. S., Kneib J.-P., Dressler A., Smail I., Czoske O., Oemler A., Natarajan P., 2003, ApJ, 591, 53  
 Trujillo I., Carretero C., Patiri S. G., 2006, ApJLett, 640, L111  
 Tully R. B., Fisher J. R., 1987, Journal of the British Astronomical Association, 98, 48

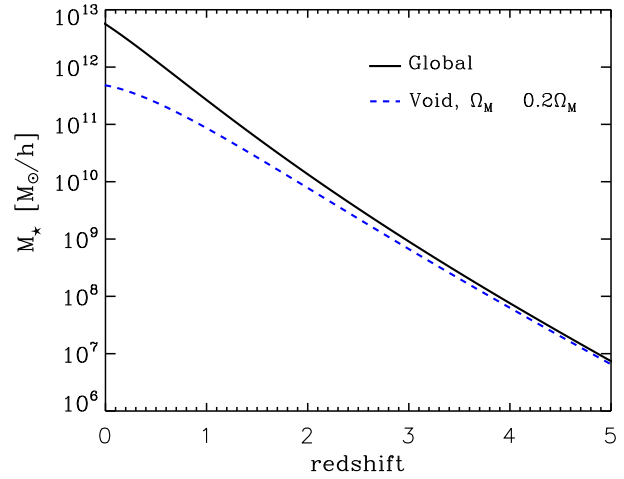


**Figure A1.**  $M_{\odot}$  as a function of redshift, both in our fiducial  $\Lambda$ CDM model, and in an approximation of a void region (see text for details).

Tully R. B., Shaya E. J., Karachentsev I. D., Courtois H. M., Kocevski D. D., Rizzi L., Peel A., 2008, ApJ, 676, 184  
 Vale A., Ostriker J. P., 2006, MNRAS, 371, 1173  
 van de Voort F., Schaye J., Booth C. M., Dalla Vecchia C., 2011, MNRAS, 415, 2782  
 van de Weygaert R., 2002, ArXiv Astrophysics e-prints  
 van de Weygaert R., van Kampen E., 1993, MNRAS, 263, 481  
 van den Bosch F. C., Aquino D., Yang X., Mo H. J., Pasquali A., McIntosh D. H., Weinmann S. M., Kang X., 2008, MNRAS, 387, 79  
 Watson D. F. et al., 2015, MNRAS, 446, 651  
 Wechsler R. H., Bullock J. S., Primack J. R., Kravtsov A. V., Dekel A., 2002, ApJ, 568, 52  
 Wegner G., Haynes M. P., Giovanelli R., 1993, A&A, 105, 1251  
 Weinmann S. M., van den Bosch F. C., Yang X., Mo H. J., 2006, MNRAS, 366, 2  
 White S. D. M., Frenk C. S., 1991, ApJ, 379, 52  
 White S. D. M., Rees M. J., 1978, MNRAS, 183, 341  
 Wyder T. K. et al., 2007, ApJSupp, 173, 293  
 York D. G. et al., 2000, A&A, 120, 1579  
 Zel'dovich Y. B., 1970, A&A, 5, 84

## APPENDIX A: NON-LINEAR MASS AS A FUNCTION OF REDSHIFT

Figure A1 shows  $M_{\odot}(z)$ , that is, the mass within a Lagrangian sphere of size such that the variance of the linear-theory density equals  $\delta_c = 1.68$ . For this, we integrated a CAMB power spectrum with the parameters of the simulation. We also show an estimate of  $M_{\odot}(z)$  in a region that is a void at time  $z = 0$ . For the void calculation, we kept fixed the shape of the linear power spectrum, but multiplied  $\Omega_m$  by 0.2 (the fiducial density in a void region) in obtaining the growth factor;  $\sigma_8$  is effectively lower in a void at  $z = 0$ .

## APPENDIX B: SIMULATIONS AND GALAXY CATALOGS

The results presented here are based on two cosmological boxes of  $64 \text{ h}^{-1}\text{Mpc}$  and  $32 \text{ h}^{-1}\text{Mpc}$  side. Each box was run at several resolutions and including dark matter only, dark matter plus gas and with and without feedback. We assumed a  $\Lambda\text{CDM}$  cosmology with values of  $\Omega_m = 0.3$ ,  $\Omega_\Lambda = 0.7$ ,  $h = 0.73$  and  $\sigma_8 = 0.8$ , in good agreement with the latest values obtained from the Planck mission (Planck Collaboration et al. 2015). The results presented here are insensitive to small variations in the cosmological parameters. The  $64 \text{ h}^{-1}\text{Mpc}$  and  $32 \text{ h}^{-1}\text{Mpc}$  boxes were run at a mass resolution of  $1.62 \times 10^8 \text{ h}^{-1} \text{ M}_\odot$  per particle corresponding to  $512^3$  and  $256^3$  particles respectively. Several zoom resimulations were run at higher resolution for selected individual haloes at  $2.02 \times 10^7$  and  $2.53 \times 10^6 \text{ h}^{-1} \text{ M}_\odot$  per dark matter particle.

The  $64 \text{ h}^{-1}\text{Mpc}$  box was run using the sph Gadget-2 code with gas and no cooling. The  $32 \text{ h}^{-1}\text{Mpc}$  simulation box is the same box described in (Aragon-Calvo 2012) and (Aragon-Calvo & Yang 2014). Gadget-2 computes long-range gravitational forces using a particle-mesh algorithm (Hockney & Eastwood 1988) and a tree algorithm for small separations (Barnes & Hut 1986). Gas dynamics are computed using a smoothed hydrodynamics approach (Lucy 1977; Springel & Hernquist 2002). The Gadget-3 sph code used to run the simulations with star formation implements recipes for hydrodynamics and metal enrichment including stochastic star formation, SN feedback and winds (Springel & Hernquist 2003). The critical density for star formation is set to  $n_h = 0.1 \text{ cm}^{-3}$ . While more detailed star formation recipes including feedback are possible, in the present work they are not critical, as the CWD mechanisms described here are mechanical/gravitational in nature and take place outside the star-forming regions of the galaxy.

### B1 Halo catalogues

From the two simulations we computed halo/sub-halo catalogs using Friends-of-Friends (FoF) and SubFind (Davis et al. 1985; Springel et al. 2005). For both haloes and sub-haloes we generated merger trees by identifying common particles between haloes/sub-haloes in adjacent snapshots. This produced large and complex trees that were then pruned to identify their “most massive progenitor” lines. The mass at each point of the most massive progenitor line forms the mass accretion history (MAH) of the halo/sub-halo. The MAH of FoF haloes is in most cases an increasing function of time. Sub-haloes, on the other hand, tend to have more erratic MAH as a result of non-linear interactions and the particle unbinding procedure (Onions et al. 2012). One particular problem of sub-halo MAH is the decrease in mass after accretion into a larger halo as a result of mass stripping. Following a similar approach as Conroy, Wechsler & Kravtsov (2006) and Vale & Ostriker (2006) we allow the mass of a sub-halo to either remain constant or increase with time. In the case of satellite haloes with severe mass stripping this means that the satellite is implicitly assumed to retain its mass right before accretion. For consistency we applied the same procedure to the FoF haloes although they have a near monotonic increase in mass.

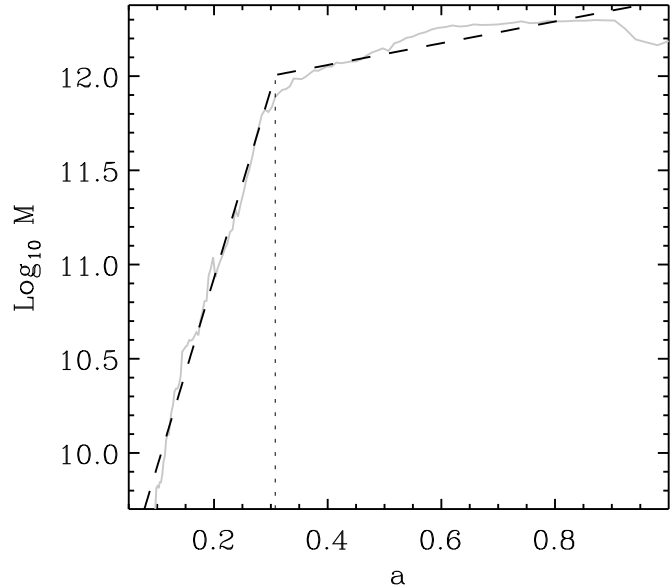


**Figure B2.** Halo mass accretion history for a sub-halo with a present time mass of  $1.5 \times 10^{12} \text{ h}^{-1} \text{ M}_\odot$  (solid grey line). The dashed line corresponds to the best two-line fit and the halo formation time (inflection point) is indicated by the vertical dotted line.

### B2 Galaxy catalogue (SDSS)

For the study of the galaxy mass-color distribution (Sec. 5.2) we used a sample of galaxies selected from the Sloan Digital Sky Survey data release 9 (York et al. 2000; Abazajian et al. 2009). We selected galaxies from the spectroscopic sample in the redshift range  $z < 0.1$  and no constraints on magnitude. Given the target selection criteria this corresponds to galaxies with a Petrosian magnitude in the red filter of  $m_r < 17.77$ . The total sample contains almost half a million galaxies which is enough to perform the matching with haloes in our  $64 \text{ h}^{-1}\text{Mpc}$  simulation at  $z = 0$ . The SDSS galaxy sample used in this work was queried from the CASJOBS service<sup>1</sup>. We selected galaxies with spectroscopic measurements in the redshift range  $z = 0 - 0.1$  using the following (abridged) query:

```
SELECT p.ObjID, p.ra, p.dec, s.z, s.zErr, s.zConf,
       s.cx, s.cy, s.cz,
       p.dered_u, p.dered_g, p.dered_r, ...
       p.petroMag_u, p.petroMag_g, p.petroMag_r, ...
       s.specclass,
       s.eClass
INTO myDB.galaxies_dr9
FROM SpecObj AS s,
     PhotoObj AS p
WHERE s.SpecObjID = p.SpecObjID AND
       s.z BETWEEN 0 and 0.1
```

<sup>1</sup> <https://skyserver.sdss.org/CasJobs>

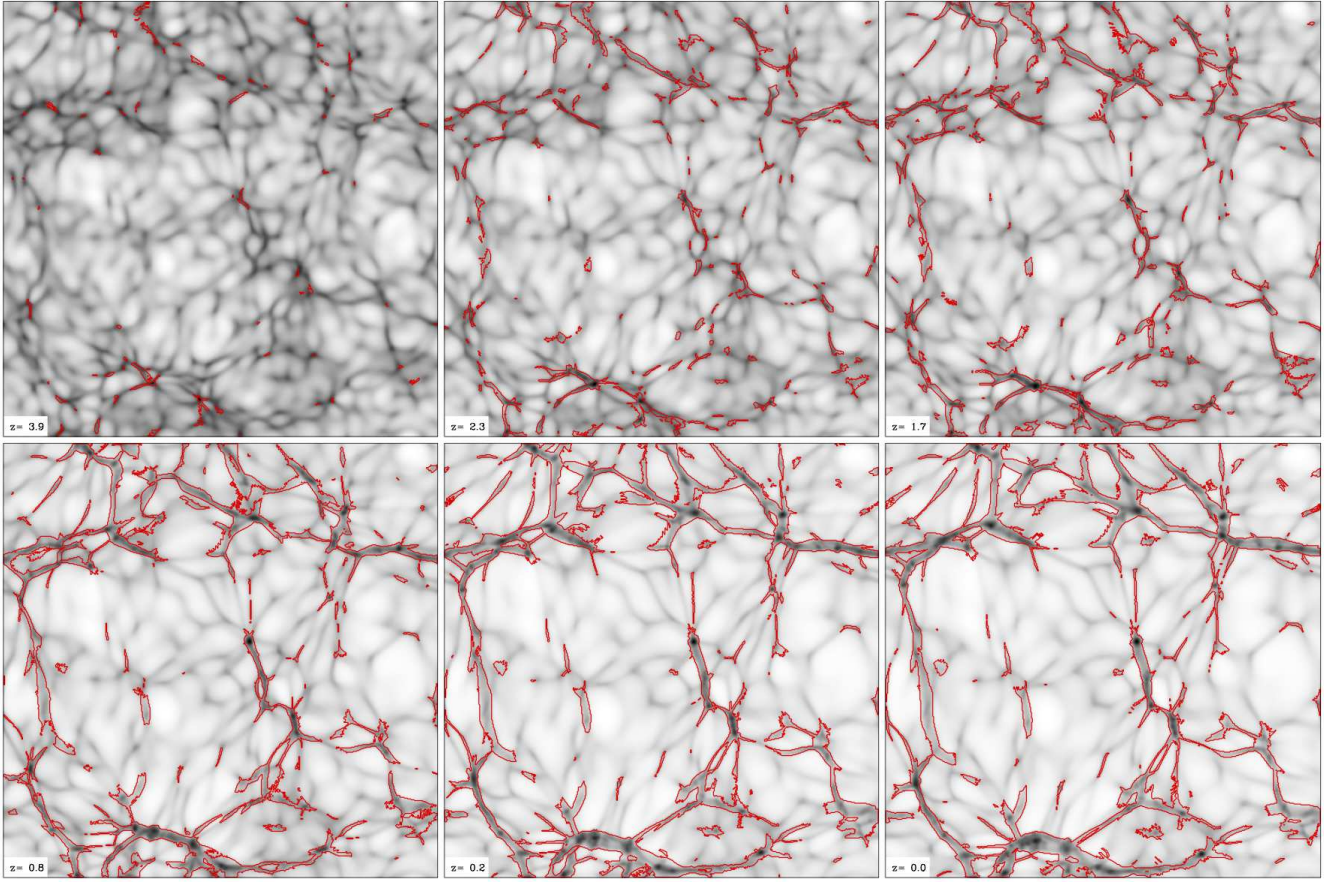


**Figure B1.** Evolution of shell-crossing regions in a  $2h^{-1}\text{Mpc}$  thick slice across the simulation box. The gray-scale background represents the projected smoothed density field. The red contours enclose the regions where shell-crossing has occurred which correspond to Web Detachment regions. This is an extended version of Fig. 5.1 in the main text.

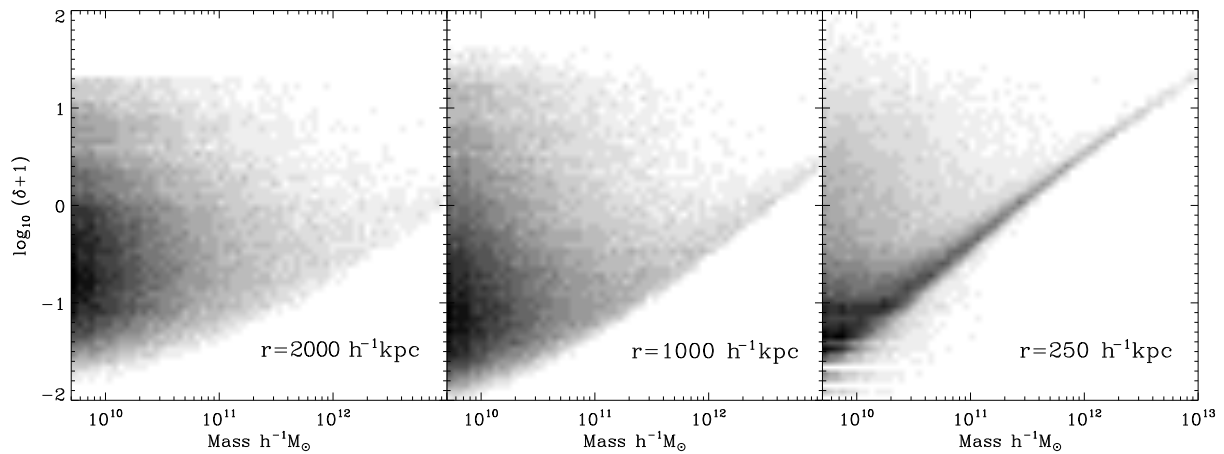


**Figure B3.** Relation between sub-halo mass and density measured inside tophat spheres of  $r = 2000, 1000$  and  $250 h^{-1}\text{kpc}$  centered on the sub-haloes. Note the envelope indicating that massive haloes do not populate low-density environments. When we measure density using smaller radius the correlation between sub-halo mass and density increases.